CHARLES UNIVERSITY

Faculty of Science

Department of Physical Geography and Geoecology

Study programme: Geography

Branch of study: Physical Geography and Geoinformatics

Eliška Sieglová

Remote Sensing of Surface Meltwater on the Glaciers of Svalbard

Tavná voda na povrchu ledovců Svalbardu studovaná metodami DPZ

Bachelor's thesis

Supervisor: Mgr. Martin Margold, Ph.D.

Prague, 2021

Prohlášení:

Prohlašuji, že jsem závěrečnou práci zpracoval/a samostatně a že jsem uvedl/a všechny použité informační zdroje a literaturu. Tato práce ani její podstatná část nebyla předložena k získání jiného nebo stejného akademického titulu.

Praha 4.5.2021

podpis studenta

PODĚKOVÁNÍ

V prvé řadě bych chtěla poděkovat mému vedoucímu práce Mgr. Martinu Margoldovi, Ph.D. za jeho ochotu, odborné vedení a za veškerý čas, který mi věnoval. Velice si cením jeho rad a připomínek a také toho, že mi umožnil zabývat se tématem, které mne zajímá. Dále děkuji také doc. Mgr. Janu Kropáčkovi, Ph.D. za konzultace týkající se metodiky práce. Také děkuji rodině a přátelům za podporu.

ABSTRACT

Supraglacial lakes pond meltwater on the surface of glaciers. They form in the ablation zone during the ablation season and their darker surface lowers the albedo of the glacier. Once drained to the glacier bed, they may affect basal sliding and flow velocities of the glacier. High-resolution imagery from the Sentinel-2 mission was used to characterize the ablation season on two glacier regions of Svalbard: Hinlopenbreen glacier on the east coast and Kongsbreen and Kronebreen glaciers on the west coast of Spitsbergen. The first supraglacial lakes appeared in the first half of June in the west region and in the second half of June in the east region. The peak of the lake area was observed around the turn of June and July in the west region and around the half of July in the east region. The time of the first appearance of supraglacial lakes corresponded with temperatures reaching positive values. They first formed in lower elevations and started progressing higher with rising temperatures. Most supraglacial lakes formed between 600 and 700 m a.s.l. in the west region and between 400 and 500 m a.s.l. in the east region. In the east region a significant number of the supraglacial lakes (12 % of their total area) formed above the estimated equilibrium line altitude of 600 m a.s.l. Further research should thus investigate what impact a warming climate has on the distribution of supraglacial lakes and on the glacier mass balance in general.

KEY WORDS:

ablation season, glacier, supraglacial lake, Svalbard

ABSTRAKT

Supraglaciální jezera se tvoří na povrchu ledovce v jeho ablační zóně. Objevují se v ablační sezóně a tmavá barva jejich vodní hladiny snižuje albedo ledovcového povrchu. Jejich odvodnění k bázi ledovce může zvýšit bazální klouzání a rychlost pohybu ledovce. S využitím snímků o vysokém rozlišení družic Sentinel-2 se tato práce zabývá charakteristikou ablační sezóny na dvou zaledněných regionech Svalbardu: území ledovce Hinlopenbreen na východním pobřeží Západního Špicberku a území ledovců Kongsbreen a Kronebreen na jeho západním pobřeží. První supraglaciální jezera se na západním území objevila v první polovině června, na východním území v druhé polovině června. Vrchol ablační sezóny byl na západním území pozorován na přelomu června a července, a na východním území v polovině července. První tvorba jezer odpovídala teplotám, které překročily 0 °C a zpočátku se tvořila v nižších nadmořských výškách. Se stoupajícími teplotami i jezera postupovala výš. Většina jezer se na západním území tvořila v nadmořských výškách mezi 600 a 700 m n. m., na východním území se tvořila zejména mezi 400 a 500 m n. m. Zde se ale nezanedbatelné množství jezer (12 % celkové plochy) vytvořilo nad odhadovanou výškou hranice rovnováhy (600 m n. m.). To vznáší otázku pro další výzkum, jaký vliv má oteplující se klima na tvorbu supraglaciálních jezer a na hmotnostní bilanci ledovců celkově.

KLÍČOVÁ SLOVA:

ablační sezóna, ledovec, supraglaciální jezero, Svalbard

TABLE OF CONTENTS

1. INTRODUCTION

Pronounced warming, thought to be of anthropogenic origin (Nordli et al., 2014), has caused glaciers to start losing large amounts of mass in recent decades. This warming has been even more noticeable in the Arctic, which is warming about twice as fast as the rest of the Earth. Glaciers are large freshwater reservoirs, and thus significantly contribute to the sea level rise of about 3.6 mm/year (Lindsey, 2021).

Surface melt of glaciers results in the formation of supraglacial meltwater channels and lakes. Their darker color, compared to snow, affects the glacier albedo and creates a positive feedback loop: the more the glacier surface melts, the more freshwater is stored in supraglacial channels and lakes, which further lowers the albedo of the glacier surface. This causes less energy to be reflected back into the atmosphere, further enhancing the melt process. Glaciers and ice sheets thus respond to climate warming in a non-linear way (Shreshta, 2011).

Glacial meltwater can either run off into the proglacial zone through supraglacial meltwater channels or, more frequently, drain through crevasses or moulins to the glacier base. Meltwater at the glacier base may enhance basal sliding and flow velocities of the glacier, as well as increase calving rates of tidewater glaciers, thus directly contributing to the sea level rise.

In this field of study, most attention is focused on the ice sheets of Greenland and Antarctica. These two ice sheets are the largest bodies of ice on Earth, the Greenland Ice Sheet contains 7.42 m of sea level equivalent (SLE) (Morlighem et al., 2017), and the Antarctic Ice Sheet contains 57.9 SLE (Rignot et al., 2019). Outside of Greenland and Antarctica, the small glaciers and ice caps only contain an estimated 0.32 m SLE altogether (Farinotti et al., 2019). However, glaciers and ice caps are the ice bodies that are the most exposed to melting and they currently contribute to the sea level rise at a similar rate as both the Greenland Ice Sheet and the Antarctic Ice Sheet (Oppenheimer et al., 2019).

Studies on supraglacial hydrology conducted on the Greenland Ice Sheet and the Antarctic Ice Sheet are the starting point for this thesis, which aims to characterize the ablation season and its effects on the glaciers of Svalbard: The study is carried out for large outlet glaciers in two areas of Spitsbergen, the largest island of the archipelago; the study area on the west coast contains the glaciers Kongsbreen and Kronebreen, and the study area on the east coast features the glacier Hinlopenbreen. Remote sensing methods are employed to study the development

and distribution of supraglacial lakes in these two regions. The aim is to inspect the inter-annual differences and the differences between the two regions and set them into context with climatic conditions.

2. THE PHYSICAL GEOGRAPHY OF SVALBARD

Svalbard is a Norwegian archipelago in the High Arctic located on the northwestern edge of the Barents Shelf. The archipelago comprises islands and islets between 74°-81°N latitude and 10°-34°E longitude with a total area of 60 667 km^2. There are four main islands with an area over 1 000 km^2, the largest of them is called Spitsbergen with the area of 37 503 km^2, followed by Nordaustlandet, Edgeøya and Barentsøya (Dallmann, 2015).

The northernmost point is on the island of Rossøya at 80°49′44.41″ N, the easternmost point is Kræmerpynten on the island of Kvitøya at 33°30'59" E, the southernmost point is a small island Keilhauøya at 19°03'18" E and the westernmost point is Fuglehuken on the island of Prins Karls Forland at 10°27'35" E. The highest point of Svalbard is Newtontoppen (1 713 m above sea level) on the Island of Spitsbergen (Figure 1).

Figure 1 - Topographic map of Svalbard. Retrieved from mappery.com.

2.1. Geology

The stratigraphy of Svalbard can be divided into basement, consisting of strongly metamorphosed rocks, and overlying layers of sedimentary rocks. Svalbard was beneath sea level for most of its geological history, which allowed for long-term activity of sedimentary processes. During this time the climate changed and affected these processes.

Svalbard's geological history has been thoroughly described in numerous scientific publications by many (Hjelle, 1993; Dallmann, 2015; Elvevold, Dallmann, Blomeier, 2007) which agree on the main points. It started in the Archaean age; the oldest rocks are 3.2 billion years old, mostly individual minerals found in metamorphic or intrusive rocks. Rocks of the basement were formed in the Precambrian age. These are mainly gneisses and granitoid intrusive rocks and they are the oldest rocks found on Svalbard today. The basement is exposed in Ny-Friesland, on the west coast of Spitsbergen, in the northern part of Nordaustlandet and on the islands Kvitøya and Bjørnøya.

In the Paleozoic age, then, Svalbard was affected by the Caledonian orogeny during the Ordovician, Silurian and Devonian. Resources further report that it was a time of folding and faulting, rocks were recrystallized and deformed, and therefore rocks from this period are metamorphosed. Today they are exposed in Ny-Friesland, on the west coast of Spitsbergen and in the northern part of Nordaustlandet.

However, most rocks exposed on Svalbard are of sedimentary origin including sandstone, shale, limestone, and dolomite. Red sandstones of Devonian age are exposed in Northern Spitsbergen, indicating an arid and hot climate in the Devonian. In the Carboniferous and Permian ages Svalbard had a tropical or subtropical climate with various forms of life. That resulted in the deposition of carboniferous sandstones including coal seams in central Spitsbergen. One of the Russian settlements – Pyramiden – was established for the purposes of mining this coal. Coal mines existed also in the other settlements such as Longyearbyen and Barentsburg and coal mining was up until recently the main economic activity in Svalbard.

The Mesozoic is described as the era when the uplift of Svalbard began. There was also volcanic activity at the sea bottom, and thus from this era there are sedimentary, volcanic and intrusive rocks. Today they are exposed in Kong Karls Land and on Spitsbergen.

Further on, in Paleogene, the northeasterly movement of Greenland caused the development of a major depression known as the Central Tertiary Basin, where heavy sedimentation took place. From this period there are coal seams in Longyearbyen, Barentsburg and Sveagruva on the island of Spitsbergen today.

In Neogene, volcanic activity was present in Northwestern Svalbard. Today there is evidence of this volcanic activity in the Bockfjorden Volcanic Complex with volcanic pools and small volcanoes.

2.2. Climate

The most important factors that affect the climate of Svalbard are its high latitude, the exchange of waters between the Arctic and Atlantic Oceans, and the North Atlantic Oscillation.

Svalbard lies in the Fram Strait which means that it is affected by the water exchange between the Arctic and Atlantic oceans. The North Atlantic Current brings warm waters of the Gulf Stream as the Norwegian Atlantic Current which follows the Scandinavian coast. The Norwegian Atlantic Current breaks up into two branches at the continental shelf edge. One branch continues east to the Barents Sea through the Bear Island Trough and the other north as the West Spitsbergen Current (Hanssen-Bauer et al., 2019). This current causes the climate around Svalbard to be milder than other regions at these latitudes.

The West Spitsbergen Current plays a very important role in the climate of Svalbard. It brings warm waters to the west coast of Svalbard, making the west coast significantly warmer than the rest of the archipelago (Copernicus Climate Change Service, 2017). It also leaves the sea south and west of the archipelago ice free even during winter (Ice Service charts, 2020).

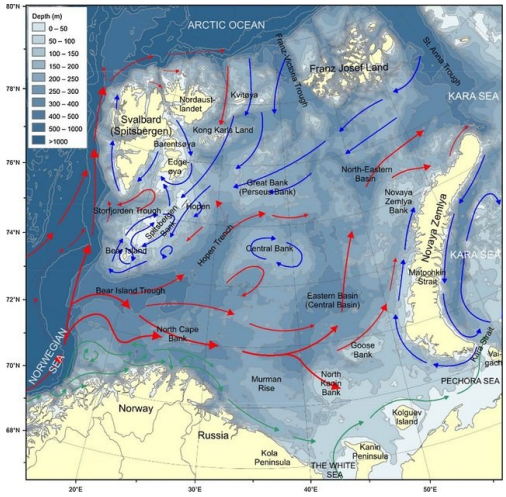

Figure 2 - Ocean circulation in the Barents Sea. Retrieved from Grosvik et al. (2018).

Information about the climate of Svalbard in the past comes from ice cores (Isaksson et al., 2003) and lacustrine sediments. Even today, defining the climate of Svalbard is not easy. There are 15 weather stations in the archipelago but all of them are situated in low elevations with coastal climate. Most of them are on the west coast which means that the climate data are highly affected by the West Spitsbergen Current. Therefore, it is difficult to estimate average values for the main climate characteristics of Svalbard and most of these average data for the whole archipelago are derived from numerical models (reanalysis data; Hanssen-Bauer et al., 2019)

2.2.1. Holocene climate

At about 10 000 years BP, during the transition from the Younger Dryas (a stadial of the last glacial period) to the Holocene, the glaciers started retreating and during the period from about 9000 BP to 4400 BP glaciers were considerably reduced compared to the later Neoglacial (Svendsen, Mangerud 1997). The last 1500 years have seen climate shifts of the Medieval Climate Anomaly (warm) and the Little Ice Age (cold).

According to Mann et al. (2009), the Medieval Climate Anomaly was a warmer period in the Northern Hemisphere observed between the years 950 and 1250 A.D., which has been linked to the occurrence of La Niña in the Pacific. According to D'Andrea et al. (2012), in the 14th century an overall cooling of the Earth began and lasted to the 18th or 19th century. This period is called the Little Ice Age because during this time glaciers exceeded their previous Holocene extents.

The occurrence of the Little Ice Age is linked to the changes in the North Atlantic Oscillation bringing precipitation to Svalbard via the West Svalbard Current (Mann et al., 2009). During the Little Ice Age the North Atlantic Oscillation was in its positive phase, which means there was low pressure above the North Atlantic that brought many winter storms (Dickson et al., 2000). According to D'Andrea et al., the glacier advance in Svalbard during the Little Ice Age was mainly caused by high precipitation during winter rather than by cold summer temperatures.

2.2.2. Climatic variables

During the last 100 years large climate fluctuations were observed. Nordli et al. (2014) used data from the Svalbard Airport composite series that began in 1911 and extended this series by data from polar hunters and research groups back to 1898. These data are however not continuous – the weather station at Svalbard Airport was established in 1975, the data before this year are taken from various sites of polar hunters' and researchers' cabins and homogenized to fit the composite. Also, the Svalbard Airport weather station was moved due to the thermal influence of the near proximity of the airport. The extended temperature series can be seen in Figure 3.

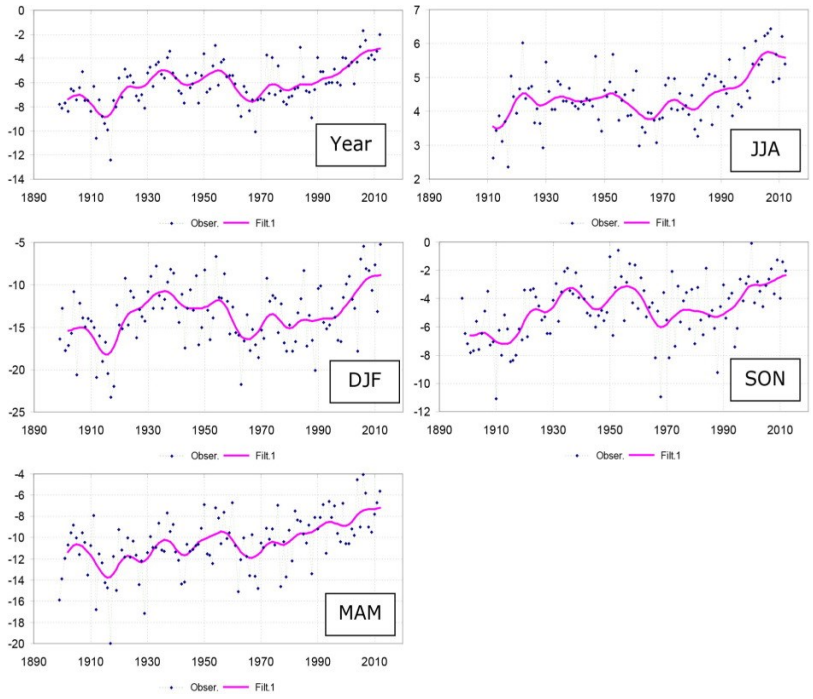

Figure 3 - Temperature records from 1898 to 2012 at Svalbard airport. Annual means (Year), Summer mean (JJA), Winter mean (DJF), Autumn mean (SON), Spring mean (MAM). Retrieved from Nordli et al. (2014).

The reconstructed temperature series of Nordli et al. (2014) display a marked period of cooling at the beginning of the 20th century centered around the year 1910. This was followed by a warmer period known as the Early 20th Century Warming (Nordli et al., 2014) which again fell into a cooler stage before 1970. After 1970 there is a clear and continuous warming which is considered to be of anthropogenic origin *"in combination with other driving factors"* (Nordli et al., 2014, p. 2).

Records from the period between 1898 and 2012 are very important for the explanation of today's climate and for future projections. Due to the remoteness of Svalbard, there were and still are not enough weather stations to allow for a full understanding of its climate as a whole. The first weather station was established in 1911 and later others have been established, however none of the series are continuous. Operations of many stations were interrupted by the war and were at some point moved to a different location due to anthropogenic changes in the environment, such as the one at Svalbard Airport (construction of an airport) or in Barentsburg (construction of a building; Nordli et al., 2014).

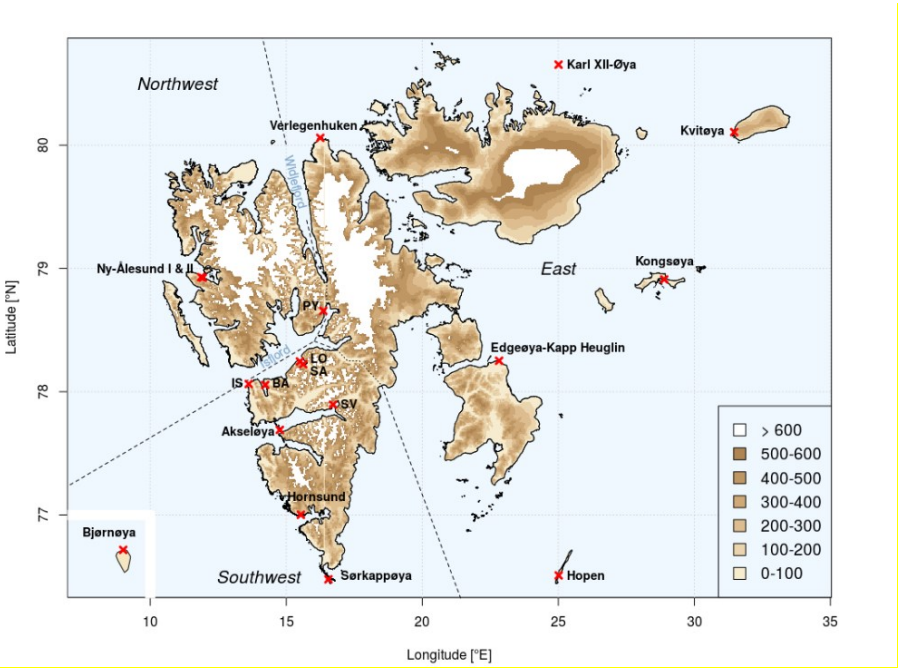

Figure 4 - Map of Svalbard weather stations (marked by a red cross). Retrieved from NCCS report no. 4/2019 (Vikhamar-Schuler et al., 2019).

Another problem when estimating the climate of Svalbard is the spatial distribution of the weather stations (see Figure 4). All weather stations are located near the coast, most of them on the west coast. There is therefore limited knowledge about the climate of the parts of Svalbard

with no weather stations, such as the inland. However, numerical models can be used to project climate for these regions.

2.2.2.1. Climatic variables (last 100 years)

According to the *Climate 2100* report of the Norwegian Environment Agency from Hanssen-Bauer et al. (2019), *"the estimated average temperature for Svalbard land areas is -8.7°C"*, with the highest average measured on Bjornoya (-1.7°C), the southernmost island, and the lowest at Svalbard Airport (-5.7°C) for the years 1971-2000. From 1971 to 2017 a warming can be seen in the records, varying between 3-5°C in different regions (Hanssen-Bauer et al., 2019) with an average warming of 0.8°C per decade (Pelt et al., 2016). The greatest changes occur in the north and the season with the highest temperature change is winter (Hanssen-Bauer et al., 2019).

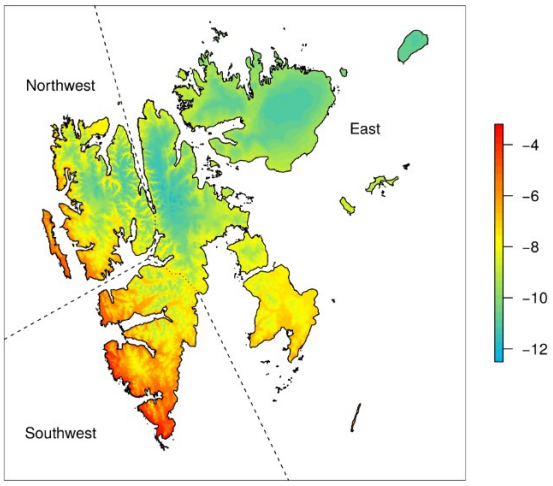

Figure 5 - Temperature map of Svalbard. "Long-term average of annual temperature in◦C (averaged over 1971-2000) from the Sval-Imp data set". Retrieved from NCCS report no. 4/2019 (Vikhamar-Schuler et al., 2019).

2.2.2.2. Climatic variables: Precipitation

When recording and calculating precipitation means a similar problem occurs. The rainfall average varies between 196 mm (Svalbard Airport) and 581 mm (Barentsburg) in the period from 1971 to 2000. The modeled average for Svalbard is 720 mm (Hanssen-Bauer et al., 2019), taking into consideration that rainfall increases with elevation. But Hanssen-Bauer et al. (2019) state that with all weather stations located in low altitudes the model results can be overestimated. In the last decades a shift in precipitation has been observed, namely that the

intensity and frequency of episodes with heavy rainfalls has increased (Hanssen-Bauer et al., 2019).

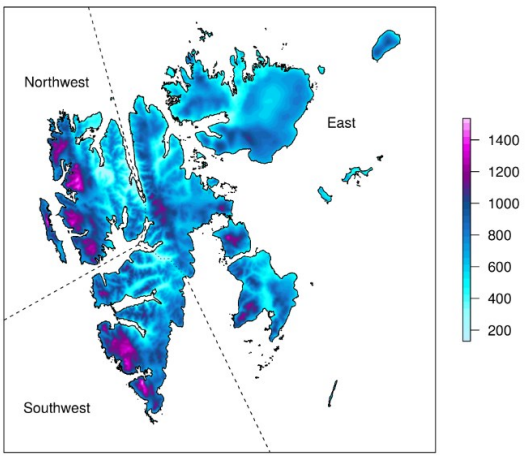

Figure 6 - Precipitation map of Svalbard. "Average annual precipitation (1971-2000) in mm from the Sval-Imp data set", Retrieved from NCCS report no. 4/2019 (Vikhamar-Schuler et al., 2019).

2.2.2.3. Climatic variables: Snow cover

The onset of snow cover is dependent on autumn temperatures and precipitation. On average the snow onset date delayed by 1.8 days per decade during the time period between 1961 and 2012 (Pelt et al., 2016). The snow disappearance date in spring is affected mainly by winter precipitation and snow accumulation. The changes in this date are not significant, averaging 0.7 days per decade over the whole archipelago (Pelt et al., 2016).

The snow onset date and the snow disappearance date determine the length of the snow duration. According to the Climate 2100 record of the Norwegian Environmental Agency, there has been a decrease of 20 days in the snow duration during the period 1958-2017 (Hanssen-Bauer et al., 2019).

2.2.2.4. Sea ice regime

As stated above, the sea ice regime is considerably affected by the West Spitsbergen Current. The warm waters brought to Svalbard's west coast prevent sea ice formation in the south and west seas of the archipelago, as well as in the fjords.

Today, the High Arctic is experiencing a climate shift due to global warming and the northern Barents Sea is considered to be the place with the greatest sea ice loss in the entire Arctic (Lind, Ingvaldsen, Tore, 2018), which is visible in Figure 7.

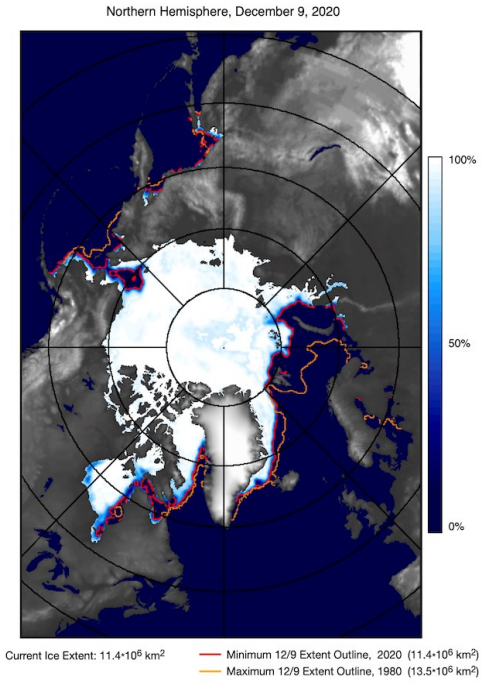

Figure 7 - Arctic sea ice extent. Comparison of years maximum 12/9 extent outline in years 1980 (orange) and 2020 (red). Retrieved from Comiso et al., (2020).

2.2.2.5. Future projections

The Norwegian Environment Agency made a report in which they projected likely changes in climate for the time interval from 1971-2000 and 2071-2100. These projected changes are as follows.

Increase in air temperature (annual average) of 7-10°C, increase of precipitation (annual average) between 45-65 % and decrease of snow duration. That will lead to more frequent floods (rain-, snowmelt- and glacier melt-floods) and a significant loss of glacier mass (Hanssen-Bauer et al., 2019).

2.3. Biota

Svalbard is located in the polar region defined as *"regions in the vicinity of the poles, where the mean temperature of the warmest month is less than 10°C"* (Thomas et al., 2008, p. 17). The polar region is thus delineated by 10°C July isotherm, which partly corresponds with the

Arctic Tree Line (the line above which trees are replaced by shrubs) and the Arctic Circle at 66°33′48.4″ N.

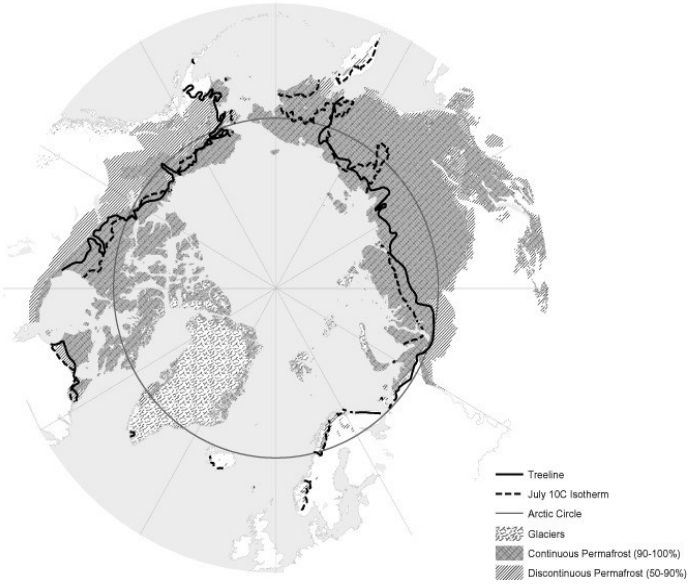

Figure 8 - Map of the Arctic polar region defined by the Polar Circle, Tree Line, and 10°C July Isotherm. Retrieved from D'Odorico et al. (2013).

With its area of 60 667 km^2, only about 36 000 km^2 of the archipelago is not covered by glaciers. Out of these 36 000 km^2 about 25 000 km^2 of the area is covered by permafrost. Permafrost is defined as any ground which maintains a temperature lower than 0°C (e.g. frozen ground) for at least two years (Humlum et al., 2003). In the summer the upper part of permafrost thaws, this upper thawed layer is called the "active layer" and can be up to tens of centimeters deep (Dobiński, 2020). Svalbard falls under the ET category of the Köppen Geiger Climate Classification: the polar tundra (Kottek et al., 2006).

Sources agree (Hansen, Hansson, Norris, 1996; Hisdal, 1998) on the description of the species living in Svalbard. The biota of Svalbard is subject to many stress factors. First of all, it is the changing photoperiod – the changing of "dark" and "light" seasons, the so-called Polar Nights and Polar Days, which means about 3 months of permanent darkness and about 3 months of permanent daylight throughout the year. Even though the climate of Svalbard is relatively mild compared to other regions at the same latitude, the estimated average annual temperature of the archipelago is -8.7°C (Hanssen-Bauer et al., 2019), which is also an important stress factor. In combination of these stress factors, the largest limiting factor in the Arctic is the survival of winter.

The fauna and flora of both terrestrial and marine ecosystems, according to Hansen, Hansson, Norris (1996) and Hisdal (1998), have mechanisms developed for dealing with these stress factors. Many arctic species are generalists, which means they use several food sources and several survival strategies. Due to the harsh conditions, there is small biodiversity, populations are also small and there is low competition between species as well as individuals.

In the marine ecosystems, temperature fluctuations are most observable in the upper water column. Most of the arctic marine species are to be found in the benthic zone at the sea bottom. Their coping mechanism for dealing with cold temperatures is to stay at the sea bottom in an inactive state during cooler periods, and contrary to pelagic species they do not need antifreeze. The pelagic species have glycoproteins in their blood that work as antifreeze components because they come in contact with temperatures below the freezing point.

The marine ecosystem is tightly bound together with the terrestrial ecosystem as there is large energy exchange between them. The most important primary producers in the ocean are plant algae (phytoplankton) that create biomass using solar energy and inorganic nutrients. Phytoplankton is the main food source for zooplankton, which creates a link between the primary producers and higher organisms like fish, seabirds, seals or whales, and also the terrestrial ecosystem. Larger fish are a food source for larger marine mammals and sea birds, the most common larger fish in the Arctic waters around Svalbard is the Arctic Cod *(Boreogadus saida)*. There are also many species of marine mammals feeding on them, the most common being: killer whales *(Orcinus orca)*, blue whales *(Balaenoptera musculus)*, narwhals *(Monodon monoceros)* or white-beaked dolphins *(Lagenorhynchus albirostris)* (Hansen, Hansson, Norris, 1996).

Animals connecting the ocean ecosystems with the terrestrial ones are species of sea birds, and mammals inhabiting coastal areas, such as walrus *(Odobenus rosmarus)* or seal species, the most common being the ringed seal, bearded seal *(Erignathus barbatus)* or harp seal *(Phoca groenlandica)* (Hansen, Hansson, Norris, 1996).

As stated before, according to Hansen, Hansson, Norris (1996) and Hisdal (1996), terrestrial ecosystems on Svalbard are highly affected by cold temperatures, permafrost and a growing period of a maximum of 3 months. Life is possible thanks to the thawing of the active layer in the summer, but only low plants occur. Plants inhabiting the archipelago are usually low with creeping structures, bowl-shaped flowers and are often found in tussocks to catch and save heat

from the sun. They must be able to photosynthesize at about 0°C and with very little insects that would assist pollination they mostly reproduce asexually or vegetatively (Hansen, Hansson, Norris, 1996). The typical flora growing on Svalbard is the Arctic white heather *(Cassiope tetragona)* and the White dryad *(Dryas octopetala)* (Hansen, Hansson, Norris, 1996).

With very little flora biodiversity, there is also a very small biodiversity of fauna. About 1 000 species of invertebrates have been recorded on the archipelago (Coulson, 2020), which is a very small number compared to more southern regions. The animal species of Svalbard often have a long lifespan, they have a small number of offspring but reproduce often, as the offspring mortality is high. The mammals often have a large body volume compared to their surface, i.e. large and round bodies, and are covered by layers of fat, blubber or fur as a coping mechanism against the cold temperatures.

The Svalbard reindeer *(Rangifer tarandus platyrhynchus)* are the only herbivore inhabiting the archipelago. They are endemic to the archipelago and have no predator. Another typical mammal for Svalbard is the polar bear, a carnivore at the top of the food web. There are about 3000 polar bears roaming the archipelago and they mainly feed on fish and mammals inhabiting coastal areas, such as walruses and seals. Another carnivorous species inhabiting the islands is the Arctic fox *(Vulpes lagopus)* (Hansen, Hansson, Norris, 1996).

The animals inhabiting Svalbard can have several different survival strategies: a) remain active in the Arctic all year round; b) stay in the Arctic all year round but are only active in summer; c) stay in the Arctic only in summer.

Animals of the first group must be adapted to extremely cold weathers, representatives of this group can be polar bears and other terrestrial mammals, and some birds (Hansen, Hansson, Norris, 1996). Terrestrial invertebrates are representatives of the second group, and the third group are usually birds, fish and sea mammals. An example of a migratory bird is the Arctic tern *(Sterna paradisaea)* making yearly journeys from the Arctic to the Antarctic and back (Hansen, Hansson, Norris, 1996).

3. GLACIERS

Glaciers are bodies of ice that result from long-term accumulation of snow and its gradual increasing density. When snow accumulates and does not melt for a whole annual cycle, the freshly accumulated snow creates pressure on the older layers leading to the reorganization of crystals, displacing air bubbles and an increase in density. Snow turns into firn after about one year, when the density of the snowpack reaches 0.55 g/cm^3. Snow is transformed into compact ice when the density reaches 84 g/cm^3 (Synek, Petránek, Smetana, 2007). The process of glacier creation usually takes hundreds of years and is conditioned by higher accumulation than ablation (National Snow and Ice Data Center, 2020b). Glaciers can only emerge and exist under specific climatic and topographic conditions. They form in areas with low temperatures and where yearly snowfall is higher than the yearly melt. Most glaciers are located in high elevations or high latitudes where the conditions are ideal (Singh, 2001). In mountain areas their occurrence is influenced by the elevation of the snowline, in high latitudes glaciers occur even at sea level.

3.1. Thermal regimes

Glaciers can be categorized either based on their thermal regime or by their morphological characteristics. Based on their thermal regime they can be classified into temperate, poly-thermal (or subpolar) and polar according to the Ahlmann classification from 1935 (Ahlmann, 1935).

Temperate glaciers are at the pressure melting point throughout their whole mass, which indicates the presence of liquid water throughout the whole glacier body. This supports movement in the glacier, making it more prone to deformations. These glaciers are also prone to basal sliding and high velocities due to meltwater at the glacier base (Fountain, 2011). Geographically they can be found from the tropical to the subpolar regions, typically being valley glaciers in mountainous areas.

Polar glaciers are the inverse of temperate glaciers. They have a cold base and their temperature is below freezing point throughout their whole mass, with surface melt occurring only during the summer season. The glacier base is frozen to the bedrock which limits basal sliding. These glaciers are found in high latitudes where the temperatures are low throughout the whole year (Singh, 2001).

The sub-polar, or polythermal, glaciers have a mixed basal thermal regime, with areas below the freezing point and areas above the melting point. Typically, they are valley glaciers where the thin margins are frozen to the bedrock, and where large pressure in the inner parts causes these parts to have a temperature above the pressure-melting point. They are typical for the Arctic regions such as Svalbard or the Canadian Arctic (Glasser, 2011).

3.2. Glacier types

The largest bodies of glacier ice are called ice sheets. They are of continental scale covering more than 50 000 km^2. Today two ice sheets exist on Earth: the Greenland Ice Sheet and the Antarctic Ice Sheet. According to Morlighem (2017, 2019), the ice thickness of the Antarctic Ice Sheet reaches over 4 000 m, the thickness of the Greenland Ice Sheet reaches over 3 000 m. These two ice sheets contain more than 99 % of Earth's freshwater ice and both together contain almost 70 m sea level equivalent.

Ice sheets cover large areas of continents and their edges are marked by ice streams and ice shelves. Ice streams are areas within an ice mass that are faster flowing then their surroundings (Ravindra, Chaturvedi, 2011). Ice shelves are floating masses of ice on water that occur when an ice sheet spreads onto the ocean. Today ice shelves are only found around the Antarctic Ice Sheet (Jenkins, 2011).

Masses of ice covering less than 50 000 km^2 are called ice caps. They form in regions at high latitudes and high elevations that are relatively flat. Ice caps can be found for example in Iceland. Ice fields are smaller than ice caps, usually comprising of interconnected glaciers. They are influenced by the topography they cover, which steers their flow. Ice fields are located in mountainous areas, one of them being Patagonia (National Snow and Ice Data Center, 2020a).

In mountainous areas, mountain (or alpine) glaciers occur. The largest mountain glaciers can be found in Canada, Alaska, the Andes or in the Himalaya. They often flow out of ice fields covering the mountain range.

Valley glaciers have a tongue-like shape and are limited by valley walls. Valley or outlet glaciers that flow down to the sea level and end in the ocean are called tidewater glaciers. These glaciers are subject to calving which is a process when parts of the glacier front break off and create floating ice bergs. Valley glaciers that spill out onto flat plains beyond the mountain front

are called piedmont glaciers, the largest of them being the Malaspina glacier in Alaska (Arora, 2011).

3.3. Glacier mass balance

Most Earth's glaciers accumulate mass during the winter and lose mass during the summer. The area where the net accumulation of the snow is positive, and where the glacier gains mass, is called the accumulation zone and is located in the upper parts of the glacier. The area where the net mass balance is negative, and where the glacier is losing mass, is called the ablation zone. The boundary between these two zones where the accumulation equals ablation is called the equilibrium line and its elevation is highly dependent on climatic factors such as temperature and precipitation, and on topography (Haeberli, 2011).

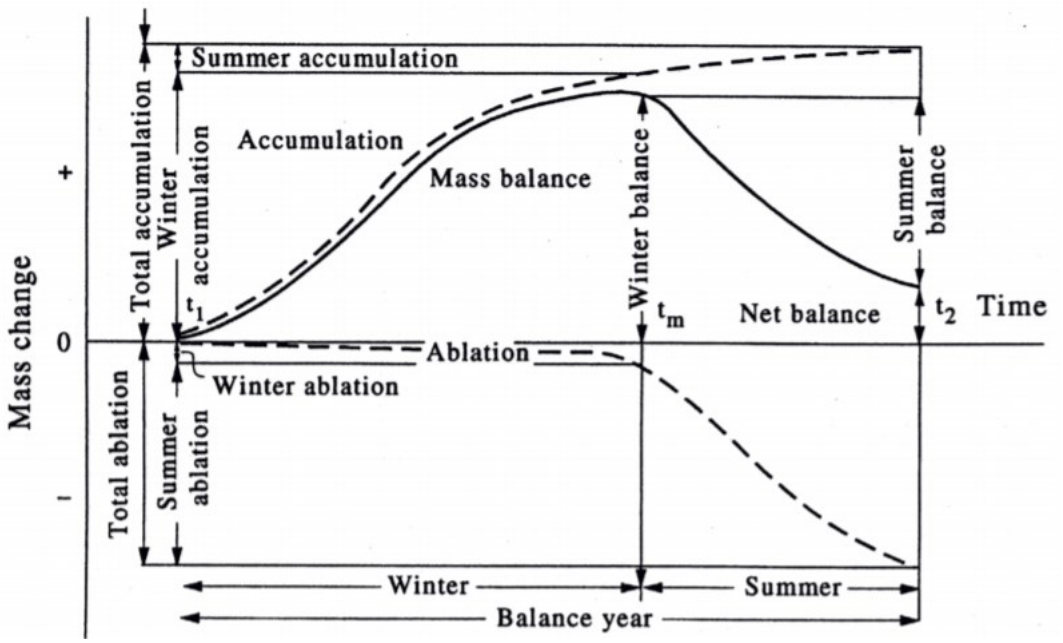

Figure 9 - Variation of accumulation, ablation, and mass balance during a glaciological year for a glacier with distinct accumulation and ablation season. Retrieved from Hock (2010).

3.4. Glacier hydrology

The study of glacier hydrology focuses on water storage and transport within a glacier. In mountain areas glacier-fed rivers are an important source of water for agriculture or hydroelectric power plants, and they may also present natural hazards such as when their courses are followed by mudflows or floods associated with drainage of glacier-dammed lakes.

Glaciers also have a large impact on the Earth's energy balance and highly affect its climate by complex interactions with the atmosphere (Shrestha, 2011).

The scale of surface melting is affected by the energy balance. A vast majority of Earth's glaciers accumulate mass during the winter season when temperatures are low and solar irradiance rates are reduced, only tropical glaciers accumulate mass during the summer months. For most glaciers the surface energy balance is positive during the summer season due to high incoming solar radiation and high temperatures, which initiates melting (Hock, 2005). Therefore, the highest runoff rates occur during the warmest and driest periods of the year, and correlate positively with air temperature. Albedo also highly affects the surface melt. Dirty snow has an albedo of 0.1 whereas the albedo of fresh snow is 0.9 (Hock, 2005).

Water can occur anywhere throughout the glacier: at the surface as supraglacial meltwater, within the glacier in englacial channels, and at the glacier base as subglacial meltwater. The water at the glacier base affects the basal sliding of the glacier. At the Greenland ice sheet the ice velocities accelerate during the summer season (Zwally, 2002).

At the beginning of the ablation season the glacier surface starts to melt when the surface energy balance turns positive. The meltwater percolates through underlying layers of snow and refreezes, thus creating an impermeable layer of ice (Pitcher, Smith, 2019). When the snowpack and firn on the glacier surface become saturated, meltwater accumulates on the glacier surface and is stored in slush zones (>15 % water content) or supraglacial lakes (Hodgkins, 1997; Pitcher, Smith, 2019). According to Irvine-Fynn et al. (2017), supraglacial lakes form in local topographic depressions in the ablation zone in areas with low surface gradient and are transient. They usually form early during the melt season and persist for 14-60 days, as observed on non-temperate valley glaciers in Svalbard, however, supraglacial lakes on ice sheets may persist even over the winter season (Irvine-Fynn et al., 2017). Water from the glacier surface can either be transported through supraglacial streams into the proglacial region or it can drain into englacial conduits through crevasses or circular vertical shafts called moulins. The water is transported to the glacier base where it affects the glacier velocities as well as the geomorphology of the glacier base. In Greenland it has been observed (Zwally, 2002) that glacial sliding is enhanced during the summer ablation season and is affected by the transport of meltwater from the surface to the ice-bedrock interface. Water from the glacier base emerges

into proglacial streams, rivers and lakes and later drains in sediment-rich plumes into the ocean (Chu, 2013).

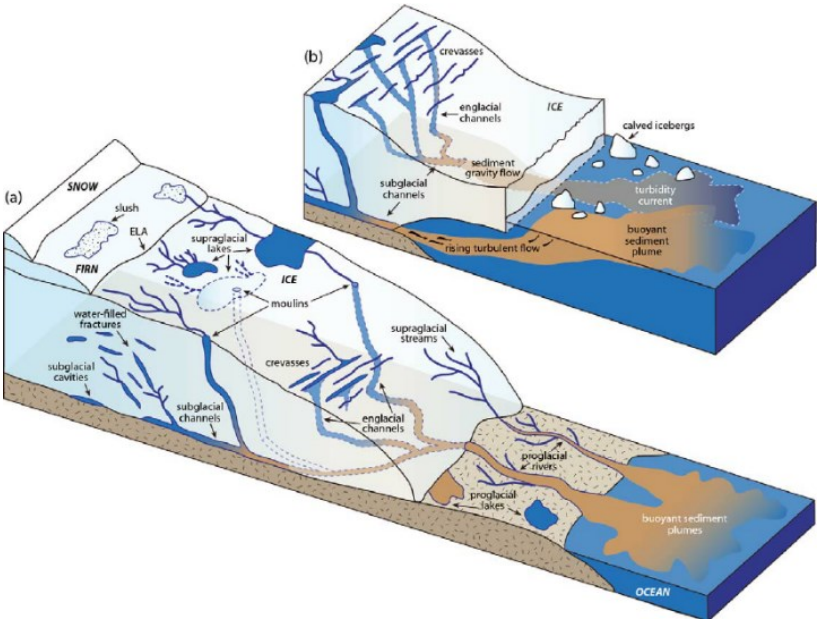

Figure 10 - The Greenland ice sheet hydrologic system of (a) land- and (b) marine-terminating glaciers. Retrieved from Chu (2014)

3.5. Glaciers and climate change

A healthy glacier accumulates the same amount of mass as it loses, however, today's glaciers are found to be losing their mass in most regions. According to the data of the World Glacier Monitoring Service (2021) the global mass change of glaciers from 1961/2 to 2015/16 was -9.625 Gt (362.5 Gt = 1 mm SLE) and the mass loss of today's glaciers is accelerating. Their possible contribution to the sea level rise is worrisome, as only the Greenland ice sheet holds about 7.2 m SLE and could contribute between 5 and 33 cm to the global sea level by 2100 (Aschwanden et al., 2019).

The response of glaciers to climate change is a very complex chain of processes (Shrestha, 2011). The mass and energy balance of the glacier surface reacts to changes in atmospheric conditions such as temperature, precipitation, solar irradiance etc.

Changes of climate in polar regions can have effects on the climate of the whole Earth because of positive feedback effect that could enhance the warming. These feedback loops are called the polar amplification and the energy exchange between ice and the atmosphere plays a main role (National Snow and Ice Data Center, 2020c). A snow- or ice-covered surface reflects about

90 % of solar radiation back into the atmosphere, whereas water absorbs most of the energy, reflecting only 6 % (National Snow and Ice Data Center, 2020c). The consequence of temperature increase is also the increase of glacier and sea ice melt, which opens large areas of open water. That darkens the ice surface, more energy is absorbed, which further increases melt and mass loss (Irvine-Fynn et al., 2017).

This can also be seen on the temperature anomalies being higher in West Antarctica and in the Arctic region (see Figure 11).

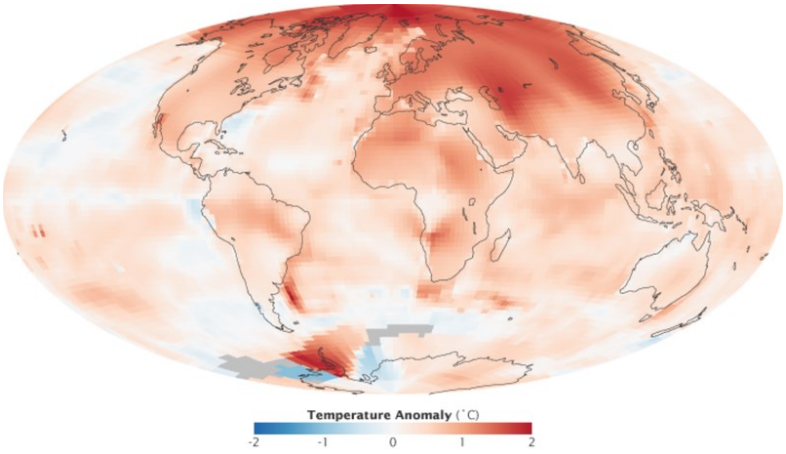

Figure 11 - Temperature anomaly between 2000 and 2009 (NASA image by Robert Simmon, based on GISS surface temperature analysis data including ship and buoy data from the Hadley Centre).

3.6. Glaciers of Svalbard

Today about 59 % of Svalbard is covered by glaciers which takes up about 35 000 km^2 (Dallmann, 2015). All the main islands (Spitsbergen, Nordaustlandet, Edgeøya, Barentsøya, Kvitøya) are partly or entirely covered by glaciers.

The distribution of glaciers depends on local climatic and topographic conditions. The presence of glaciers correlates positively with winter precipitation. Dry regions have less glaciated area than regions with higher precipitation (Dallmann, 2015).

Spitsbergen is a mountainous island and is mostly covered by ice fields with intervening mountain ridges. There are three main ice fields on Spitsbergen: the northwest, northeast and southeast. On the other hand, islands to the northeast of Spitsbergen are flat and covered by ice caps. The largest ice caps are called Austfonna (8357 km^2) and Vestfonna (2402 km^2) and both lie on the island Nordaustlandet (Dallmann, 2015). On the island Prins Karls Forland some typical piedmont glaciers, can be found (Hagen, 1993).

Over two thirds of Svalbard's glaciers are tidewater glaciers.The largest tidewater drainages are from the ice caps on Nordaustlandet, Austfonna and Vestfonna, and from the ice fields along the east and west coast of Spitsbergen (Dallmann, 2015). There are no ice shelves in Svalbard, as all marine-terminating glaciers are grounded at the ice front (Hagen, 1993).

While some of the small cirque glaciers in the north belong to the polar type, most glaciers of Svalbard are subpolar, or polythermal. Their characteristic is that they are non-temperate (their temperature is beneath the freezing point) in most of their mass but at their base they are temperate and with the occurrence of liquid water (Hodgkins, 1997). The margins of these glaciers are frozen to the ground. Overall, the flow rate of Svalbard glaciers is low, and thus the occurrence of crevasses is also low. A typical phenomenon is the summer melting which creates a supraglacial drainage system with meltwater channels and lakes on the glacier surface (Hagen, 1993). According to Hodgkins (1997, p. 962), the annual ablation season at Svalbard begins in late May and *"the mean distribution of runoff by month was: May, 0.8%, June, 17.4%, July 46.4%, August, 33.2%, and September 2.2%"* (as of the year 1992).

Since the 1930s the glaciers of Svalbard are marked by a dramatic retreat (Hagen, 1993; Dallmann, 2015). Based on aerial photography, the average yearly retreat of glacier fronts is between 30-40 m (Dallmann, 2015). In addition, measurements of mass balance indicate the thinning of glaciers. The year is divided into the accumulation (winter) season and ablation (summer) season, measurements for comparisons of mass balance changes during these seasons are made in spring and autumn. Glacier mass balance then reflects the loss or gain of glacier mass over a specific time length (Hanssen-Bauer et al., 2019). Negative mass balance occurs when the winter accumulation is smaller than summer ablation. For Svalbard studies show a *"long-term trend towards more negative mass balance"* (Dallmann, 2015, p. 48). The total mass loss for the glaciers of Svalbard is estimated at 0.15-0.3 m water equivalent/year (Dallmann, 2015). The ice mass loss contributes about 0.015-0.03 mm/year (Dallmann, 2015) to the global sea level rise of 3.6 mm/year on average between the years 2006 and 2015 (Lindsey, 2021).

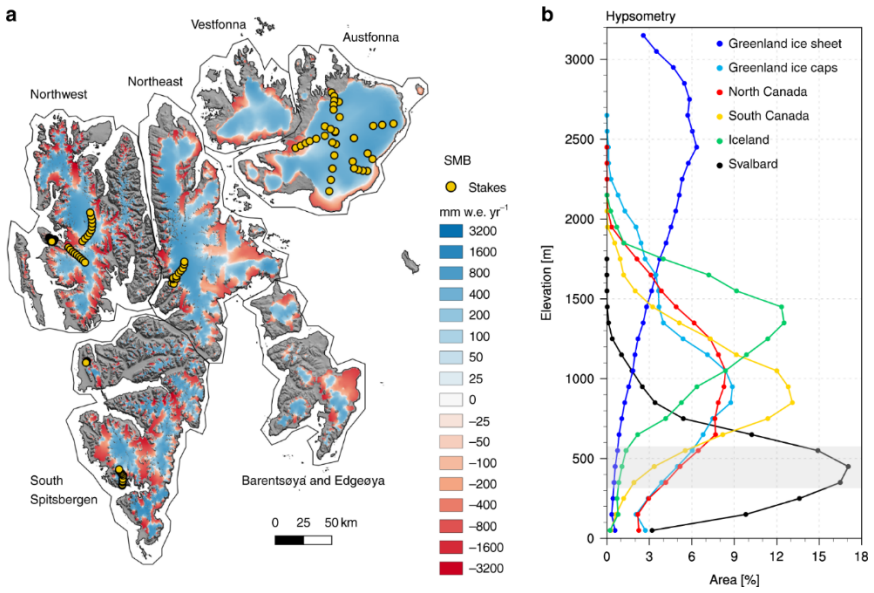

Figure 12 - Svalbard glaciers mass balance (a) and hypsometry (b). Retrieved from Noël et al., (2020).

Another indicator of glacial retreat is the increasing altitude of the equilibrium line that separates the accumulation and ablation zones of glaciers, therefore the elevation with zero mass balance. The highest Equilibrium Line Altitude (ELA), at about 800 m a.s.l., is in the central areas of Spitsbergen, where the lowest winter precipitation is measured. The ELA is lowest in the southeast of Spitsbergen at about 200 m a.s.l. (Hagen, 1993).

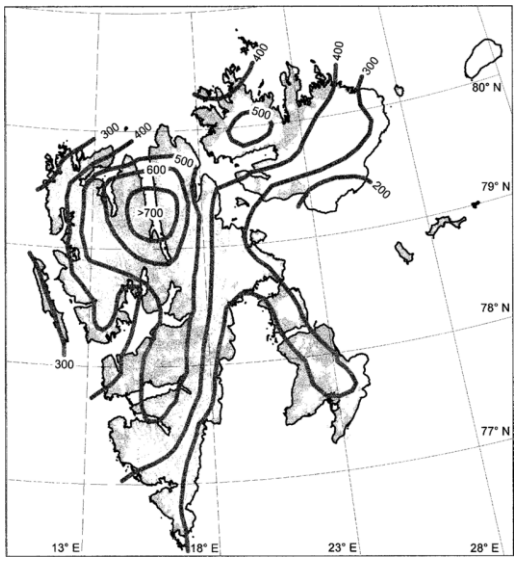

Figure 13 – The pattern of the equilibrium line altitude in Svalbard. Retrieved from Hagen et al. (2003).

The *Norwegian Environmental Association*'s report *Climate of Svalbard 2100* (Hanssen-Bauer et al., 2019) projects dramatic changes between the years 1971-2000 and 2071-2100. Due to the expected temperature increase, there is also an expected increase in the negative mass

balance during the summer ablation season, which will increase the overall negative mass balance as a consequence. The projected position of ELA is on average 400 m higher (Hanssen-Bauer et al., 2019) in the years 2071-2100 compared to the years 1971-2000.

4. STUDY AREA

Two regions, one on the west and one on the east coast of Spitsbergen, were chosen for the analysis of the ablation seasons in the years 2017 to 2020. The region on the west coast comprises the glaciers Kronebreen and Kongsbreen (further-on 'the west region'). The region on the east coast covers the area of the glacier Hinlopenbreen (further-on 'the east region'). The borders of the regions are delimited using the CryoClim "Glacier Area Outline" database and the Svalbard land boundary from the Norwegian Polar Institute database.

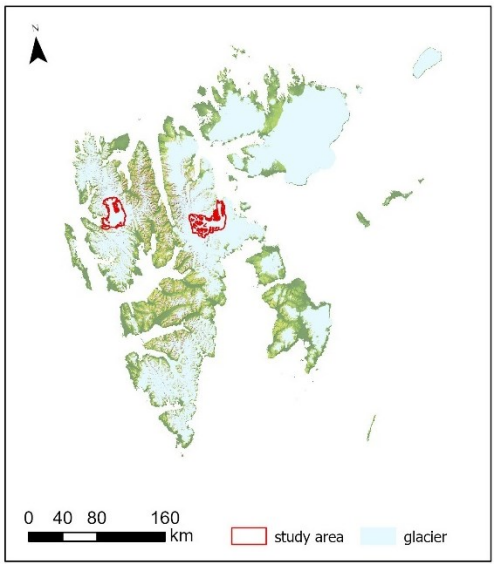

Figure 14 - The study areas on a map of Svalbard. (ArcticDEM, CryoClim).

The two regions were chosen for their location at a similar latitude and for the observed rich formation of supraglacial hydrology features during the ablation season. Both regions lie on the latitude of about 78.9°N. Both regions have a large range of elevation; from sea level to 1 448 m (west region) and 1 712 m (east region).

Hinlopenbreen (the east region) is the largest outlet glacier on Svalbard. It terminates in the sea in Hinlopenstretet. It drains an area of 1250 km^2. At its widest point the glacier is 6 km wide. In 1970 the glacier surged 2.5 km in a year, moving forward 12 m/day on average (Hagen, 2020). The highest point of the east region is at 1 712 m a.s.l. – the peak of Newtontoppen, the highest point of Svalbard. The average surface gradient of the region is 5.1°. According to Hanssen-Bauer et al. (2019) the equilibrium line altitude in the northeast part of Svalbard is about 600 m a.s.l.

The glaciers Kongsbreen and Kronebreen terminate in the innermost part of Kongsfjorden. The two glaciers drain an area of 690 km^2 and are separated by the mountain range Colletthøgda. They are 22 km long and at their widest point the glacier area is about 14 km wide. Kongsbreen and Kronebreen are glaciers with the highest registered flow velocity in Svalbard with an annual average speed of 2 m/day (Hagen, Barr, 2019). Due to that the glacier surface is crevassed. The highest point of the region is at 1 448 m a.s.l. The average surface gradient is 4.2°. According to Hanssen-Bauer et al. (2019) the equilibrium line altitude in the northwestern part of Svalbard is located about 850 m a.s.l.

Figures 15 and 16 show the regional statistics of the two study areas. The east region has a wider range of elevations than the west region, as well as a higher average surface gradient. However, the average elevation is lower than in the west region.

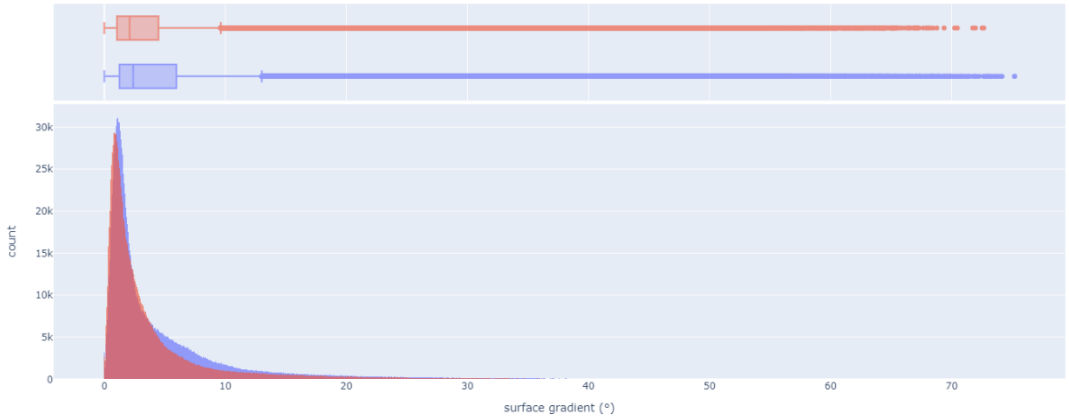

Figure 15 - Histogram and boxplots of surface gradient distribution in the east region (blue) and in the west region (red).

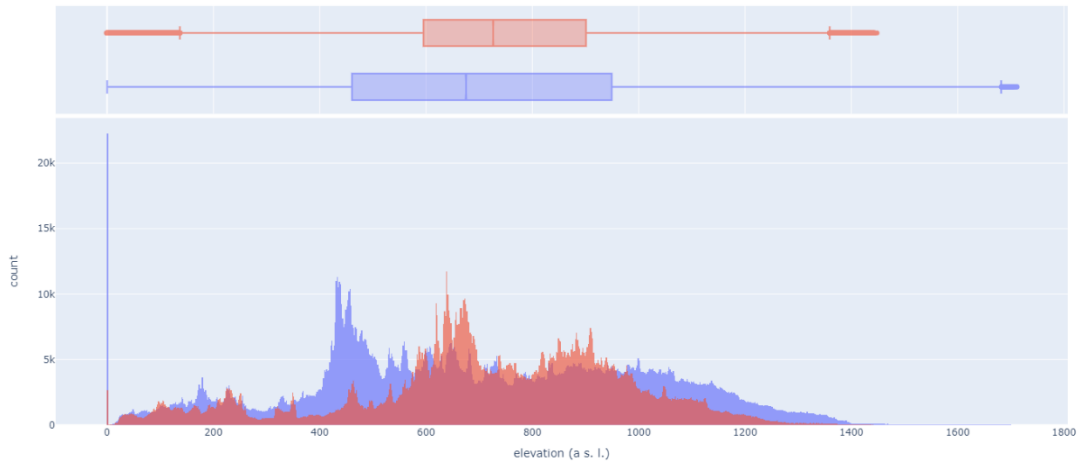

Figure 16 - Histogram and boxplots of elevation distribution in the east region (blue) and in the west region (red).

	lowest point	highest point	avg elevation	highest slope gradient(°)	average slope (°)
Kongsbreen and Kronebreen (West)	0	1 448	714	72.7	4.2
Hinlopenbreen (East)	0	1 712	696	75.2	5.1

Table 1 - Regional characteristics of the study areas.

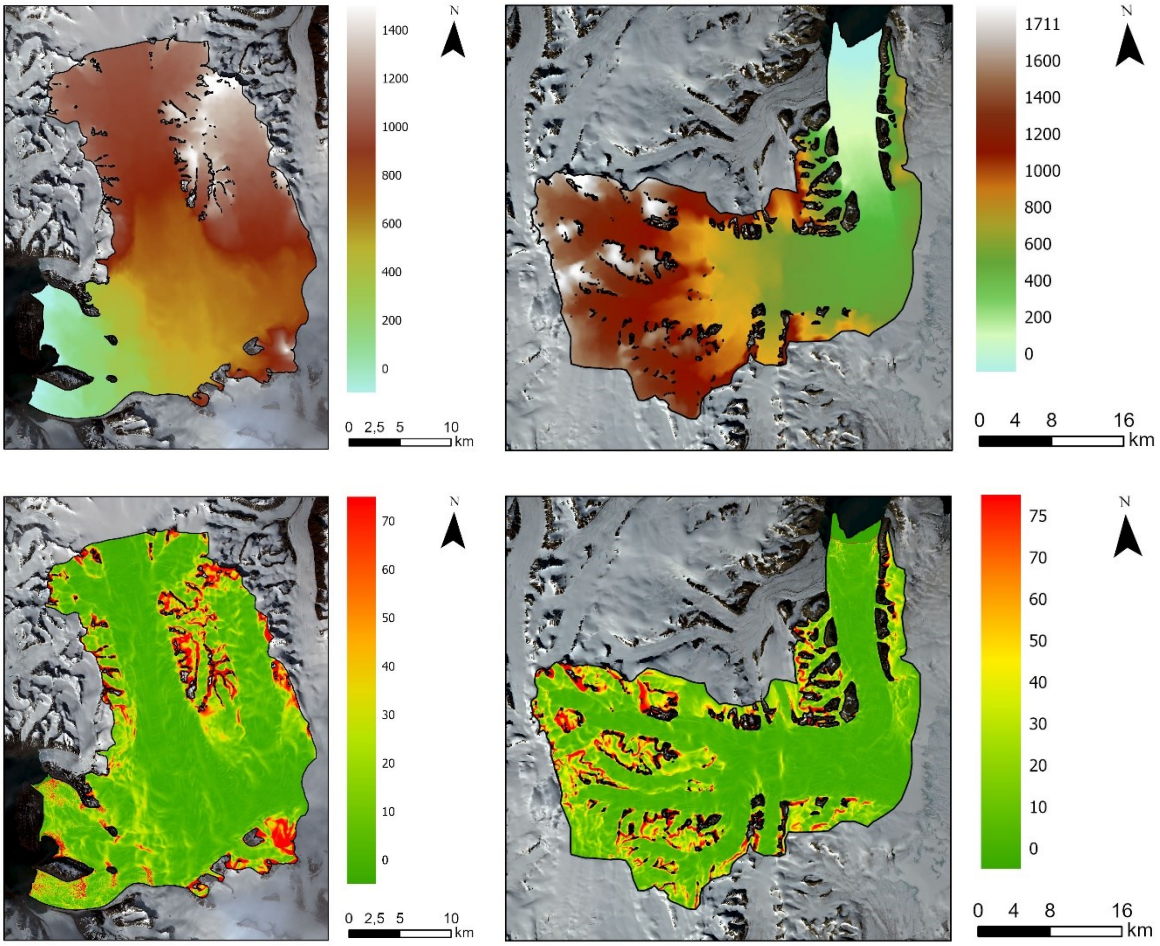

Figure 17 - Elevation in m (top) and surface gradients in ° (bottom) of the study areas: Kongsbreen and Kronebreen (left), Hinlopenbreen (right). Maps were created with Sentinel-2 (ESA) satellite images, ArcticDEM elevation data (Polar Geospatial Center), "Glacier Area Outline" database (CryoClim) and Svalbard land boundary (Norwegian Polar Institute).

5. HYPOTHESIS

The main goal of this thesis is to develop an algorithm that will detect water bodies and distinguish them from snow and slush zones on the glacier surface using Sentinel-2 satellite imagery.

The formation of supraglacial lakes is dependent on the climate and topography and the course of the ablation season highly correlates with temperatures. Because the temperatures reach positive values around the beginning of June, it can be assumed that the first supraglacial meltwater will emerge around this time. The temperatures reach a peak on average at the turn of July and August so that will supposedly be the time of the most meltwater on the glacier surface.

The climate on the west coast is milder, therefore it can be assumed that the ablation season will have an earlier onset. On the other hand, the temperatures maxima reach higher values in the east region, therefore it can be assumed that the supraglacial hydrology system will be better developed. Because the ELA in the west region is higher, it is expected that the supraglacial lakes will form in higher elevations than in the east region.

6. METHODS

6.1. Temperature measurements

In this thesis data from the ERA5 database of the Copernicus Climate Change Service (2021) are used for the comparison of temperature rates in the two study areas. As stated above, the coverage of Svalbard with weather stations is insufficient and ERA5 provides temperature models based on atmospheric variables. The data cover the whole Earth and comes in rasterized format with a spatial resolution of 30 km per pixel. The temperatures are given in degrees Kelvin, for conversion to degrees Celsius 272.15 has to be subtracted. The standard deviation of the downloaded dataset is 2.09 K.

Daily values for 2-m temperature at 12:00 were downloaded from the dataset "ERA5-Land hourly data from 1981 to present" for the period between 1981 and 2000. Attempts to download more data were made (for the hours 00:00, 06:00, 12:00, 18:00) but the downloaded dataset was too large for further processing in ArcGIS Pro. The daily data are very inconsistent with rapid temperature changes even within short time periods; therefore a weighted moving average of the data was calculated to smoothen the temperature curve.

Several parameters were tested for the visualization of the weighted average and the 30-day weighted moving average was found to have the best performance after testing several different values. It clearly shows the trends but at the same time smoothens large extremes. For the weighted moving averages of Svalbard temperatures between the years 2016 and 2020 see Supplement 1.

6.2. Data selection

With the aim to study the supraglacial hydrology cycle during the ablation season, Sentinel-2 imagery was selected among the available satellite data. Sentinel-2 provides the visible and near infra-red parts of the spectrum, which are needed for the analysis of supraglacial hydrology with the use of the normalized difference water index. Using Landsat 8 imagery was also considered but the Sentinel-2 mission was found preferable, largely thanks to the spatial resolution and revisit time of its imagery.

The revisit time of Sentinel-2 is 5 days at the equator and at high latitudes an images are available nearly every day. This is because that Sentinel-2 has two satellites in the orbit – Sentinel-2A and Sentinel-2B and also a wider swath width than the Landsat-8 (Li, Roy, 2017).

Images acquired by the Sentinel-2 mission also have very high spatial resolution – 10 m per pixel in the visible and near infra-red parts of the electromagnetic spectrum. For studying supraglacial hydrology, spatial resolution is an important factor because the width of supraglacial streams or ponds may only be a few meters. In comparison, Landsat-8 data have a lower temporal and spatial resolution (20 m). There are methods how to improve the spatial resolution, one of them being the pan-sharpening method. This method utilizes the Landsat 8 panchromatic band of a 15-m-per-pixel-resolution to increase the resolution.

However, the Sentinel-2 mission is a younger project than the Landsat-8 mission and only covers the last five years. The first Sentinel-2 satellite started to orbit the Earth in 2015. In 2016 Sentinel-2B was launched. The Landsat-8 satellite was launched in 2013, however the earlier Landsat family satellites operate since 1972 (USGS, n.d.).

Satellite	**Sentinel-2**	**Landsat 8**
Sensor	MSI	OLI
Number of bands	12	8
Spatial resolution	10, 20, 60 m	15, 30, 100 m
Revisit time	5 days (10 days for each satellite)	16 days
Swath width	290 km	185 km
Launch date	23.6.2015 (S2A), 7.3.2017 (S2B)	11.2.2013

Table 2 - Comparison of Sentinel-2 and Landsat 8 (USGS, n.d.; ESA, 2021)

The main issue encountered when collecting data was the cloud coverage. As the images were to be analyzed in the visible and near infra-red bands, acquiring images with the least possible cloud coverage was necessary. For each year it was possible to acquire only between 3 and 15 cloud-free scenes. This precluded continuous observations of the ablation seasons because for some periods the glacier surface was not visible from the satellite for several weeks. From the years for which the images were acquired, the fewest images were available for the year 2020, the most for the year 2017. An attempt to download images also for the year 2016 had to be abandoned with only a few scenes available for 2016; this was because only Sentinel-2A was in the orbit.

6.3. Image acquisition and preprocessing

The Sentinel-2 products are given in tiles covering 100x100 km^2. The tiles covering the study areas are T33XVH for the region located on the west coast and T33XWH for the region located on the east coast.

Sentinel-2 data is provided in two levels: Level-1C (L1C) and Level-2A (L2A). The measurements for the L1C products are provided in Top Of Atmosphere (TOA) reflectance. The data retrieved were of the type L1C from the USGS Earth Explorer interface (last access 17.4.2021). To carry out atmospheric corrections and to convert the L1C products to L2A products that contain information of Bottom Of Atmosphere (BOA) values, the Sen2Cor processor from ESA was used.

Further on, the imagery was processed in the program Sentinel Application Platform (SNAP) produced by ESA. The images were resampled to a resolution of 10 m per pixel. Spatial subsets and band subsets were created for reducing the data size. The spatial subset was chosen according to the area of interest. The band subset was chosen to fit the needed measurements, the bands kept in the file were B3 (green), B8 (NIR) and B11 (SWIR). These bands were further used to compute the sought indices.

6.4. Image classification

The further processing and classification of the images was also conducted in SNAP.

The goal was to classify the pixels into one of these three categories: water, snow or slush. The following indices were tested: Normalized difference water index (NDWI), normalized difference snow index (NDSI), normalized difference moisture index (NDMI) and normalized difference vegetation index (NDVI).

$$NDWI = \frac{(Green-NIR)}{(Green+NIR)}, NDSI = \frac{(Green-SWIR)}{(Green+SWIR)}, NDMI = \frac{(NIR-SWIR)}{(NIR+SWIR)}, NDWI = \frac{(NIR-Red)}{(NIR+Red)}$$

All the tested indices were based on the assumption that the pixels should be classified based on different water content. The results were compared visually with the RGB composite in natural colors.

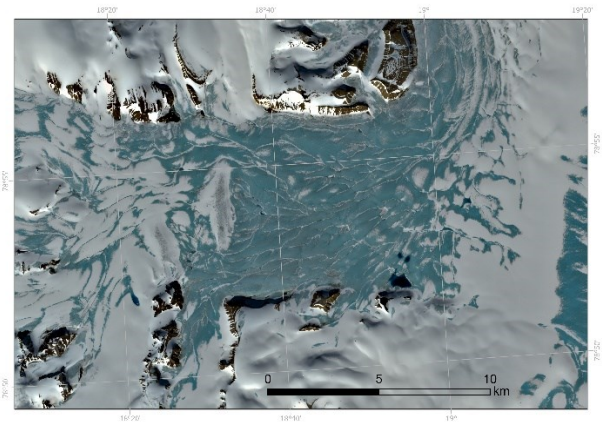

Figure 18 - Slush zone on the Hinlopenbreen glacier, 29.07.2018 (Sentinel-2 image, ESA).

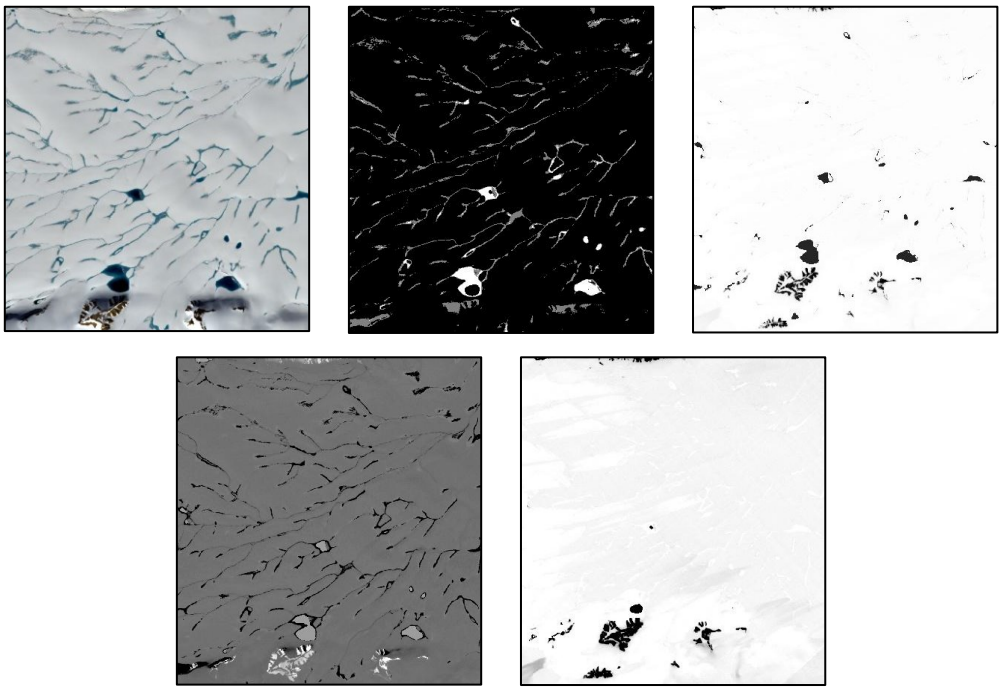

Figure 19 - RGB (upper left), NDWI (upper center), NDSI (upper right), NDMI (lower left), NDVI (lower right).

NDWI was chosen to be the main algorithm to distinguish between water, snow and slush because it clearly separates between water, snow and slush pixels (as shown on Figure 19) and because no spatial resolution was lost during the computation of this index (which would happen if bands of different spatial resolution were used). The NDWI was computed on the images using the expression (Green-NIR)/(Green+NIR); in Sentinel-2 the bands used were B3 (Green) and B8 (NIR). Both of these bands are provided in 10 m per pixel resolution.

Snow, slush and water were separated using thresholds in the NDWI values. These were determined based on visual comparison of the RGB natural color composite with the computed

NDWI. For distinguishing between water and slush the thresholds of 0.35, 0.7 and 0.9 were tested. There is no ideal threshold value that would work universally throughout the ablation season because the conditions on the glacier surface change. The lowest threshold value of 0.35 works best when there is little to no slush on the glacier and the edge between water bodies and snow is very clear. However, when this threshold value is applied to an area with slush zones, a lot of the slush is classified as water bodies. For distinguishing between water and slush a higher threshold value such as 0.7 or even 0.9 is needed. However, when this high threshold value is applied to a region with little to no slush, a large amount of data can be lost because the algorithm leaves some shallower water bodies unclassified.

The final thresholds used in this thesis are 0.9 and 0.2. Pixels with NDWI values above 0.9 are classified as liquid water, pixels with values below 0.2 are defined as snow. Pixels between these values are defined as slush. With this threshold value deep supraglacial lakes are classified as water and shallower supraglacial lakes and streams are classified as slush. During the time period when the glacier is covered by vast slush zones, some pixels representing slush are still being mistakenly classified as water. The results of the classification have to be manually corrected by removing the areas of the misclassified slush zones.

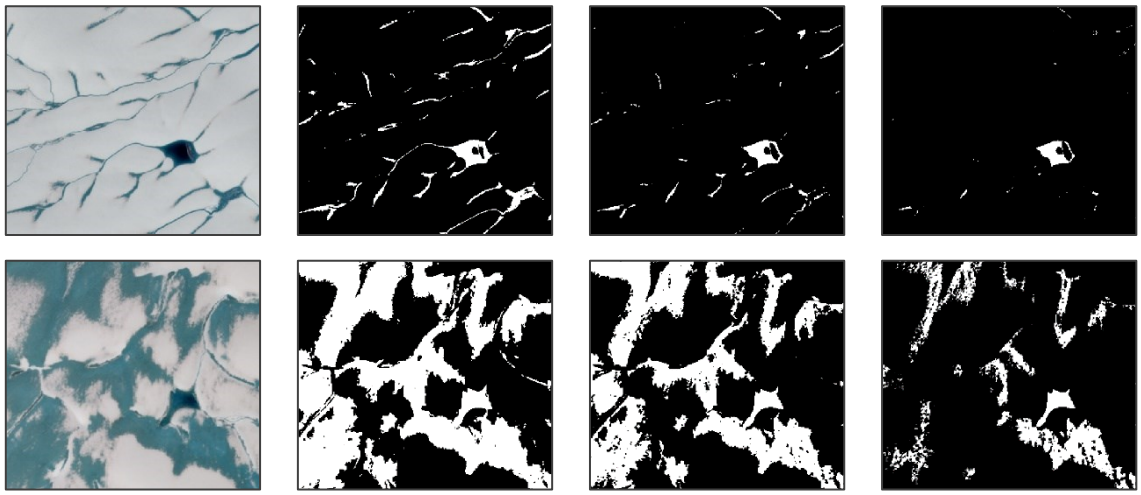

Figure 20 - Comparison of threshold values on a Sentinel-2 image from Hinlopenbreen, acquired on 13.7.2018 (upper row) and on 29.7.2018 (lower row). From left to right: RGB composite in natural colors; NDWI (threshold: 0.35); NDWI (threshold: 0.7); NDWI (threshold 0.9).

Apart from the problematic separation between water and slush, the main problem with using the NDWI is that pixels covered by clouds or shadows are often misclassified as water. For cloud detection the Braaten-Cohen-Yang cloud detection method was used. According to

Braaten, Cohen and Yang (2015) this method achieves 88% accuracy when distinguishing between water and clouds. Using this method, pixels classified as clouds were set to the value of zero (later on worked with as NoData). This method successfully eliminates cloud pixels, however, shadows cast by clouds or mountains are still being misclassified as water. Additionally, the NDVI was used to classify pixels not covered by snow using the threshold of 0.02.

The whole expression as computed in SNAP is: *if ((B11>0.2 AND ((B3 > 0.175 AND (B3-B4)/(B3+B5) > 0) OR B3>0.39))) then 0 else if ((B8-B4)/(B8+B4) >0.02) then 4 else if (B3-B8)/(B3+B8) > 0.9 then 1 else if (B3-B8)/(B3+B8) > 0.2 then 2 else 3.*

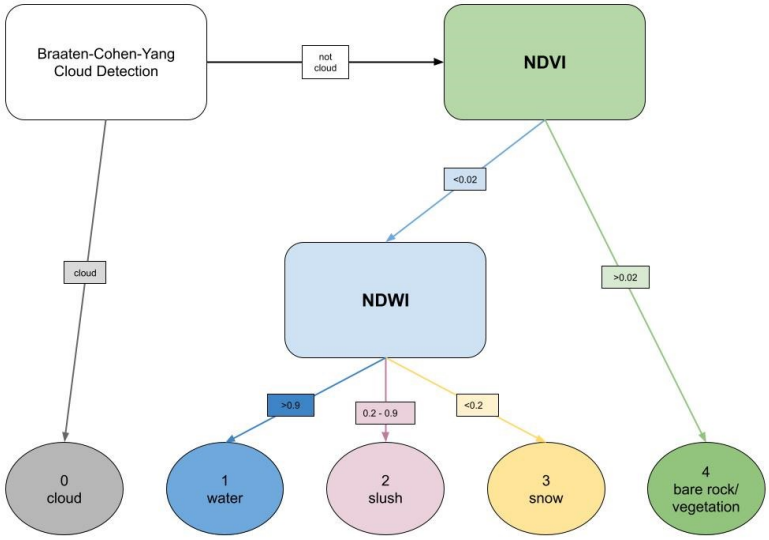

Figure 21 - The algorithm in SNAP used to classify pixels as either 0 (nodata), 1 (water), 2 (slush), 3 (snow), 4 (bare rock/vegetation).

The resulting image processed in SNAP is a raster with four values as in Table 2.

Value	Type
0	nodata
1	water
2	slush
3	snow
4	bare rock/vegetation

Table 3 - Classification of image

The classified output was exported in GeoTIFF format so that the data could be further processed in ArcGIS Pro.

6.5. Image analysis

Further processing was conducted in ArcGIS Pro to find the spatial statistics of the glacier surface. For the processing of several images a model was built in the ArcGIS Model Builder module.

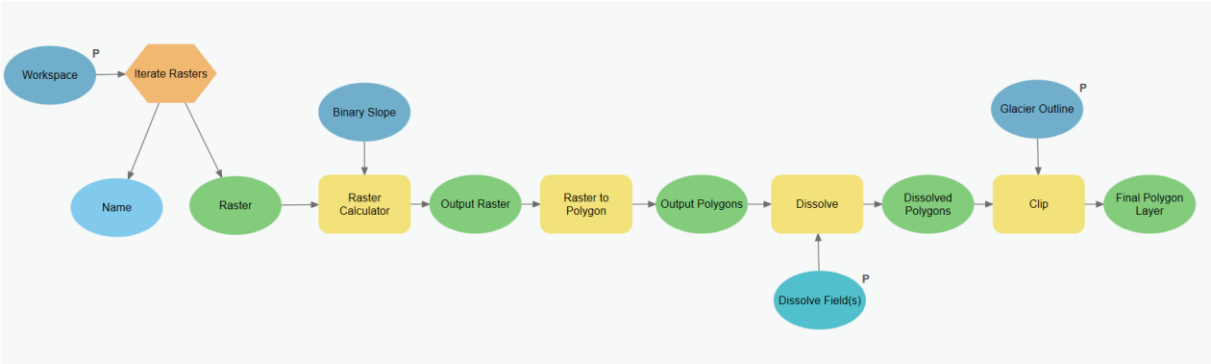

Figure 22 – First part of model for processing the raster images in ArcGIS Pro.

The input of this model is a folder where the classified images from SNAP are saved in GeoTIFF format.

The next step eliminates pixels covered by shadows that are cast by mountains because these areas are incorrectly classified as liquid water. For this, external data was needed. ArcticDEM, a digital elevation model produced by the Polar Geospatial Center, was used to retrieve information about the terrain. From this raster dataset the surface gradient was calculated using the *Slope* function in ArcGIS Pro. This was then reclassified to a binary raster with the zero value being assigned to areas with a surface gradient greater than 10° and 1 for areas with a surface gradient lower than 10°. According to Reynolds (2000), supraglacial lakes cannot exist on slopes steeper than 10°. Reynolds (2000, p. 1) writes to this topic: *"It has been found that where supraglacial lakes have formed since 1966, surface gradients of the glaciers concerned were in all cases less than 2°. At gradients of 2-10° supraglacial ponds can form but tend to be transient due to the opening and closing of crevasses."* However, the boundary of 10° surface gradient does lead to loss of information in crevassed areas.

The boundary of 10° still leads to large shadow areas being falsely classified as water or slush especially during late August and September when the Sun is lower, and the shadows cast by

mountains cover larger areas. No method was found to work effectively to eliminate the shadows properly. This needs to be considered when further working with the data.

The output raster layer as then transformed to a polygon layer so that attributes could be assigned to the classes. Using the *Dissolve* function the polygons were aggregated based on a common attribute, in this case the area type: nodata, water, slush, snow or bare rock/vegetation.

The satellite image was already cropped in SNAP when creating a subset, however, this process was only done to reduce the amount of data on which the indices were computed. To isolate an area for the ensuing analysis, the polygon layer was cropped to the glacier area outline layer (see Section 4) using the function *Clip* in ArcGIS Pro.

Because all the glaciers are marine-terminating, and are subject to calving, large areas of the ocean were classified as water in areas of 0 m a.s.l. To remove the ocean, the glacier area outline was cropped by the Svalbard land boundary before running it through the model.

Finally, the area in hectares was calculated for each class (nodata/water/slush/snow) and saved into a directory as a .CSV file.

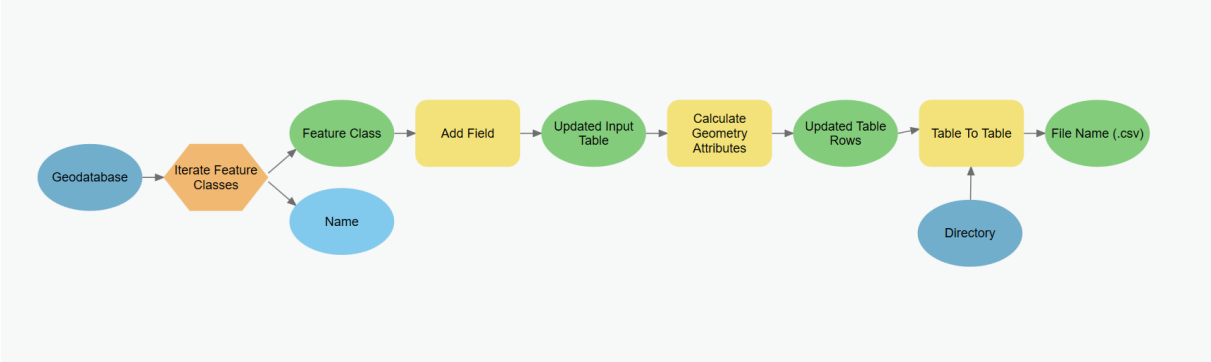

Figure 23 - Second part of model for processing the polygon layers in ArcGIS Pro.

These files contained information about the area coverage statistics used in the comparison with the temperature measurements.

6.6. Extraction of supraglacial lakes

Further on a more detailed examination of supraglacial lakes in the two study areas was done. Only polygons classified as water were extracted and the following features were investigated: the onset and peak of the melting season and the distribution of supraglacial lakes on surface gradients and elevation levels.

As stated before, many areas covered by shadows were classified as water bodies. Therefore, the outputs were visually compared with the satellite images and incorrectly classified water bodies were removed from the data.

Using the ArcticDEM and the function *Zonal Statistics as Table* in ArcGIS Pro, the information about altitude and slope gradient was extracted for each lake polygon.

6.7. Comparison of the study areas

For each region, one year was chosen for visualizing the ablation season and the formation and drainages of supraglacial lakes. The data were processed in ArcGIS Pro. For conducting a comparison it would be suitable to choose the same year for each study area. However, this was not possible because of insufficient availability of cloud-free images. The year 2019 was chosen for the west region, because of the availability of cloud-free images during the beginning and the peak of the ablation season. It was also the third warmest year since 1900 (behind 2016 and 2020; Lindsey, 2019). 12 images were acquired and processed.

Unfortunately, it was not possible to study the development of the ablation season for the same year in the east region. 11 cloud-free images were acquired, however, there was a large gap between the 20th of June and the 10th of July, which is the time period when the most supraglacial lakes form. Instead, the year 2018 was chosen for the east region.

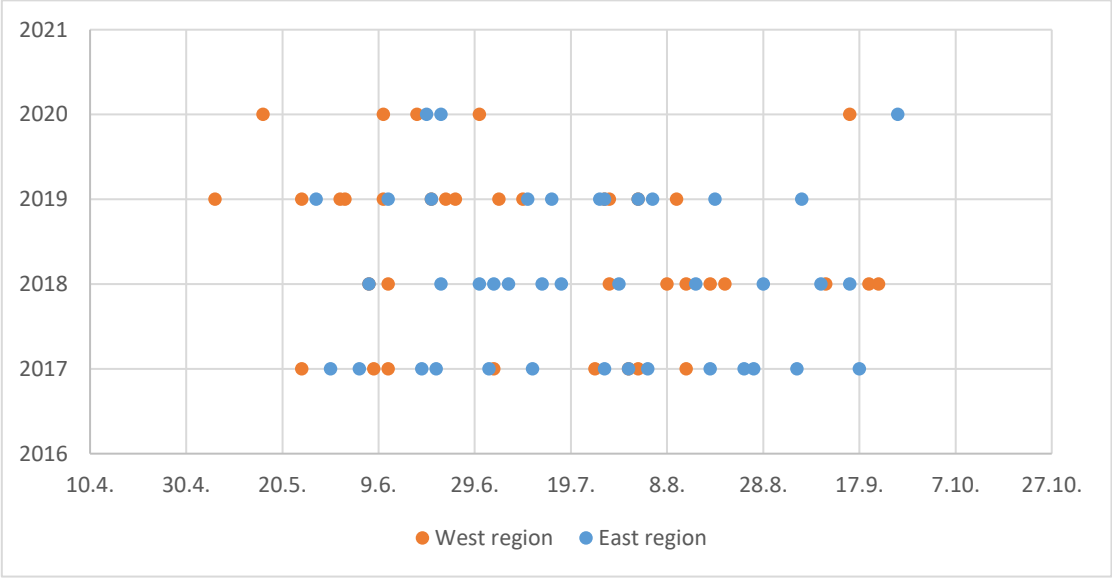

Figure 24 – Sentinel-2 images acquired for the east (blue) and west (orange) region in the years 2017, 2018, 2019 and 2020.

It was prioritized to have sufficient data for mapping the development of the ablation seasons in the two regions, even at the cost of non-identic atmospheric conditions. It was assumed that within one year, no radical changes in the distribution of supraglacial lakes will appear. The following characteristics were chosen for comparison: the beginning and peak of the ablation season, the distribution of supraglacial lakes on different elevation levels and surface gradients. Together with the knowledge of the equilibrium line altitude and the temperatures, this was put into context with the climate in both regions.

7. RESULTS

7.1. Temperature measurements

The mean summer temperatures during the years 2017-2020 were computed, and the mean temperature above Hinlopenbreen (east region) was 0.32 °C while the mean summer temperature above Kongsbreen and Kronebreen (west region) was 0.22 °C (Copernicus Climate Change Service (C3S), 2021). While the west region had slightly lower mean summer temperatures, its was somewhat milder, in suit with the stated hypothesis, with lower extremes both in winter and in summer (Copernicus Climate Change Service (C3S), 2021).

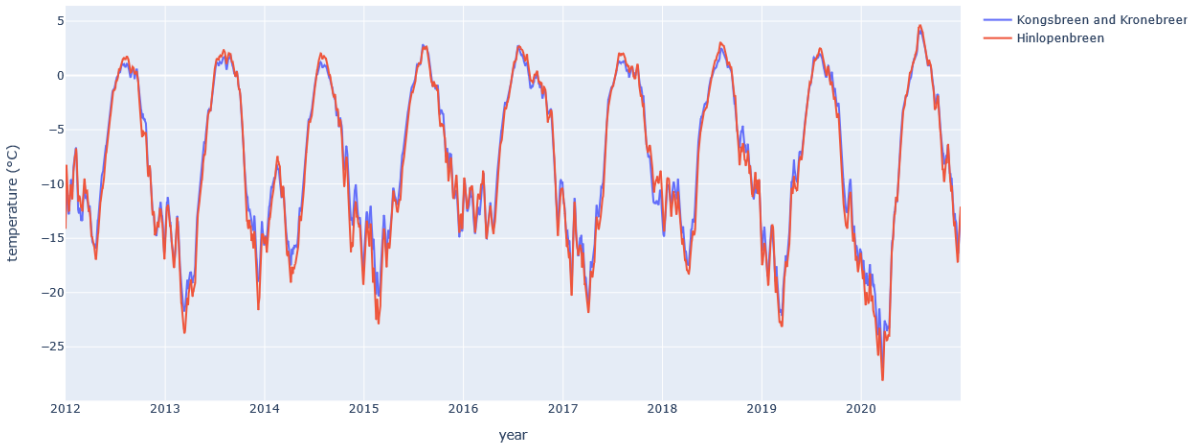

Figure 25 - Daily 12:00 temperatures for the years 2012-2020 over the area of Hochstatterbreen (blue) and Kongsbreen and Kronebreen (red). A weighted moving average of 10 days is plotted. Based on data from the ERA5-Land database (Copernicus Climate Change Service (C3S), 2021).

7.2. The ablation season of 2018 at Hinlopenbreen (East region)

The temperatures at Hinlopenbreen reached positive values in the middle of June. The formation of supraglacial lakes corresponded with the temperatures. On the 7th of June there was no meltwater present on the glacier surface and the first supraglacial lakes were observed on the 30th of June 2018 (see the map series in the Appendix for the described course of the evolution of the supraglacial lakes). On the 3rd of July first meltwater ponds appeared at the glacier edges in two regions. They were mainly concentrated in low elevations between 200 and 300 m a.s.l. (5.5 ha), and also between 500 and 600 m a.s.l. (1.4 ha). Between the 3rd and 6th of July the area of meltwater on the glacier surface tripled (from 7.9 ha to 25 ha).

On the 13th of July, the quantity of meltwater on the glacier surface was at its peak with 209 hectares of water area. On the 13th of July 94 % of the supraglacial lakes were located in

elevations between 500 and 600 m a.s.l., which indicates the drainage of most supraglacial lakes in low elevations that first emerged on the 3rd of July.

Between the 13th and 17th of July a couple of lakes drained either partly or completely, with the largest complete drainage occurring on a lake with an area of 8 hectares. On the 29th of July most supraglacial lakes were drained, however, the snow on the surface had a high water content and there appeared a vast slush zone covering 18 % of the glacier area. Most of the lake basins remained empty until the end of the ablation season.

However, one area at the elevation above 450 m a.s.l. remained undrained and three lakes even continued expanding their size (this area is highlighted in Figure 27). The largest of these lakes expanded its size from 15.9 hectares on 13.7.2018 to 93 hectares on 9.9.2018.

On the 15th of September, the whole glacier area was covered by fresh snow with no water observable.

Figure 26 – Daily 12:00 temperatures for the ablation season of 2018 at Hinlopenbreen (east region). Based on data from the ERA5-Land database (Copernicus Climate Change Service (C3S), 2021).

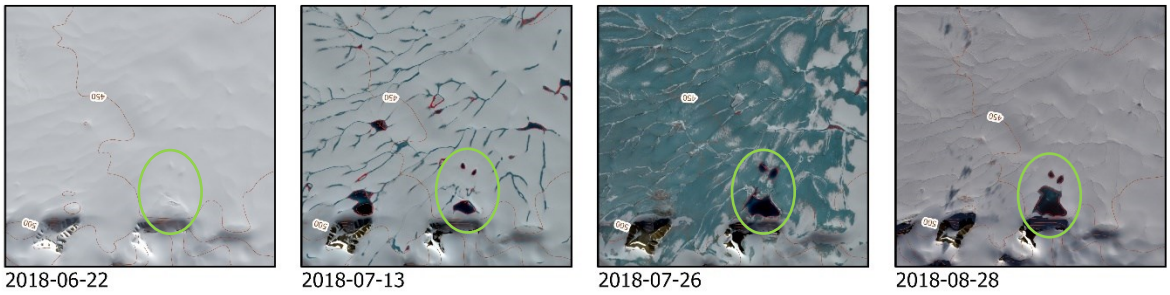

Figure 27 - The ablation season of 2018, Hinlopenbreen Red lines delineate boundaries of lakes.Green elipse highlights the largest lake that formed on Hinlopenbreen during the ablation season of 2018. It expanded from 15.9 hectares on 13.7.2018 to 93 hectares on 9.9.2018, while most other lakes already drained.

elevation \ date of image acquisition	05-25	06-22	06-30	07-03	07-06	07-13	07-17	07-29	08-14	08-28	09-09	09-15
0-100	0,00	0,00	0,00	0,52	0,00	0,00	0,00	0,00	0,00	0,00	0,00	0,00
100-200	0,00	0,00	3,84	2,61	6,89	0,00	0,00	0,00	0,00	0,00	1,56	0,00
200-300	0,00	0,00	5,77	2,87	4,49	1,11	0,00	0,07	0,00	0,00	0,00	0,00
300-400	0,00	0,00	0,68	0,04	0,58	2,30	5,53	0,11	0,00	0,00	1,54	0,00
400-500	0,00	0,00	0,00	0,84	5,02	46,52	121,82	51,09	101,10	74,62	106,37	0,00
500-600	0,00	0,00	0,00	0,59	2,67	27,07	27,97	6,30	0,00	0,00	2,79	0,00
600-700	0,00	0,00	0,00	0,00	3,07	20,34	12,07	10,78	0,00	0,00	0,18	0,00
700-800	0,00	0,00	0,00	0,00	1,19	2,27	0,00	3,00	0,00	0,11	0,15	0,00
800-900	0,00	0,00	0,00	0,00	0,00	0,24	0,00	0,07	0,00	0,00	0,00	0,00
900-1000	0,00	0,00	0,00	0,00	0,35	0,07	0,00	0,04	0,00	0,00	0,37	0,00
1000-1100	0,00	0,00	0,00	0,00	0,22	0,07	0,00	0,00	0,00	0,00	0,00	0,00
1100-1200	0,00	0,00	0,00	0,00	0,29	0,00	0,07	0,00	0,00	0,00	0,00	0,00
1200-1300	0,00	0,00	0,00	0,00	0,00	0,00	0,00	0,54	0,00	0,00	0,00	0,00
1300-1400	0,00	0,00	0,00	0,00	0,00	0,00	0,00	0,00	0,00	0,00	0,00	0,00
1400-1500	0,00	0,00	0,00	0,00	0,00	0,00	0,00	0,00	0,00	0,00	0,00	0,00
Sum	0,00	0,00	10,29	7,46	24,76	100,00	167,46	72,00	101,10	74,73	112,95	0,00

Table 4 – Area covered by water (in hectares) on elevation levels for each image acquired at Hinlopenbreen (east region) during the 2018 ablation season. First water was detected on 30.6., however, there is a lower value on 7.3. This is caused by cloud coverage of the lower elevations, where most supraglacial lakes were located at the beginning of July. Most supraglacial lakes were detected on 29.7. The values of water on the glacier surface remain high until September because of a supraglacial lake of 93 hectares at its maximum size remained undrained. The most supraglacial lakes form in elevations between 400 and 500 m a.s.l., however, their occurrence in elevations between 500 and 700 is not negligible.

7.3. The ablation season of 2019 at Kongsbreen and Kronebreen (West region)

Figure 283 – Daily 12:00 temperatures for the ablation season of 2019 for the glaciers Kongsbreen and Kronebreen (west region). Based on data from the ERA5-Land database (Copernicus Climate Change Service (C3S), 2021).

Temperatures at Kongsbreen and Kronebreen reached positive values on the 13th of June, however, first water on the glacier surface was detected on the 10th of June (2.4 ha). Because the temperatures are averaged over the whole glacier area it is possible that at sea level the temperatures were already over 0°C. 96 % of this water was located in elevations between 0 and 100 m a.s.l. Kongsbreen and Kronebreen are the fastest flowing glaciers of Svalbard, which makes their front highly crevassed up to the elevation of 450 m a.s.l. According to this, the water was probably suspended in crevasses. On the 23rd of June, more meltwater appeared even in higher elevations between 300 and 400 m a.s.l.

On the 4th of July, the ablation season was supposedly at its peak with 135 hectares of meltwater on the glacier surface. Most of the supraglacial lakes were located in elevations between 600 and 700 m a.s.l. The lakes at these elevations were numerous, but fairly small. The largest water body detected on this elevation level was 10.2 ha in area. On the 9th of July there was less meltwater (60 ha) present because of complete or partial lake drainages (see Appendix). On the subsequent image from the 26th of July, supraglacial channels were visibly empty, and 26 hectares of water remained on the glacier surface, mainly in elevations between 500 and 600 m a.s.l. Between the 26th of July and the 2nd of August no large changes occurred. On the 10th of August 10.4 ha of water was still detected on the glacier surface. Unfortunately, no other images

were acquired during this ablation season because of clouds covering large areas of the glacier surface.

elevation	date of image acquisition								
	05-26	06-02	06-10	06-23	07-04	07-09	07-26	08-02	08-10
0-100	0,00	0,00	2,01	0,00	0,00	0,07	0,00	0,00	0,00
100-200	0,00	0,00	0,07	2,88	0,00	0,04	0,00	0,04	0,00
200-300	0,00	0,00	0,00	0,00	0,00	0,00	0,00	0,00	0,00
300-400	0,00	0,00	0,00	10,57	2,27	0,00	0,00	0,00	0,00
400-500	0,00	0,00	0,00	0,70	30,55	20,32	11,16	8,82	6,61
500-600	0,00	0,00	0,00	0,00	34,19	10,82	5,18	1,42	1,86
600-700	0,00	0,00	0,00	0,00	78,07	28,96	9,26	6,31	1,95
700-800	0,00	0,00	0,00	0,00	9,36	0,00	0,00	0,00	0,00
800-900	0,00	0,00	0,07	0,00	0,00	0,00	0,00	0,00	0,00
900-1000	0,00	0,00	0,00	0,00	0,00	0,00	0,00	0,00	0,00
1000-1100	0,00	0,00	0,00	0,00	0,00	0,00	0,00	0,00	0,00
1100-1200	0,00	0,00	0,00	0,00	0,00	0,00	0,00	0,00	0,00
1200-1300	0,00	0,00	0,00	0,00	0,00	0,00	0,00	0,00	0,00
1300-1400	0,00	0,00	0,00	0,00	0,00	0,00	0,00	0,00	0,00
1400-1500	0,00	0,00	0,00	0,00	0,00	0,00	0,00	0,00	0,00
Sum	0,00	0,00	2,16	14,15	154,44	60,21	25,61	16,59	10,43

Table 5 - Area covered by water (in hectares) on elevation levels for each image acquired at Kongsbreen and Kronebreen glaciers (west region) during the 2019 ablation season. First water was detected on 10.6. in lower elevations. Most supraglacial lakes were detected on 4.7. Values of water area on the glacier surface drop rapidly because of lake drainages in elevations between 600 and 700 m a.s.l., where the most supraglacial lakes form.

7.4. Comparison of the ablation seasons at the two study areas

The distribution of supraglacial lakes on slope gradients agreed with observations of Stokes et al (2019) that they are formed in areas with low surface gradients. In both regions the majority of supraglacial lakes formed on surface gradients below 3°.

Based on data from the years 2017-2020 (Figure 29) it is visible that the ablation season begins earlier in the west region, with water detected on the glacier surface already in the first half of June. In the east region the first meltwater occurs in the second half of June. Accordingly, the peak of the ablation season is observed to come about 10 days earlier in the west region. However, this cannot be exactly specified because of the intervals between the image acquisition dates.

In both regions the formation of supraglacial lakes began in lower elevations, with more lakes appearing in higher elevations later, supposedly with rising temperatures.

In the east region at the beginning of the ablation season most supraglacial lakes were detected in elevations between 200 and 300 m a.s.l., but their overall concentration was largest between 400 and 500 m a.s.l. (85 % of the supraglacial lakes were found in these elevations). A significant number of supraglacial lakes also formed between 500 and 700 m a. s. l (10 % of the supraglacial lakes).

In the west region water is detected at even lower elevations between 0 and 200 m a.s.l., but overall, most supraglacial lakes are formed between 600 and 700 m a.s.l. (44 % of the supraglacial lakes). 46 % of the detected lakes were located in elevations between 400 and 600 m a.s.l.

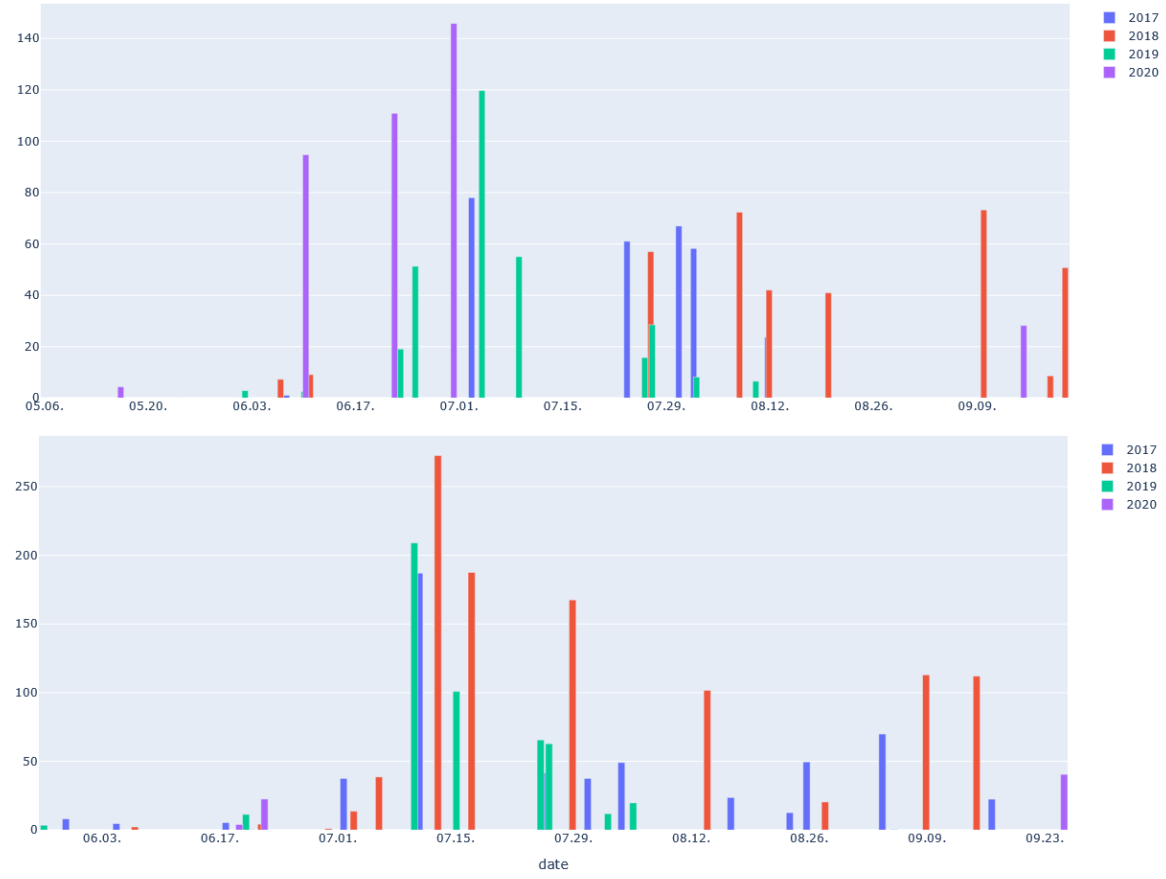

Figure 29 - Comparison of water area (ha) detected in the two regions in the years 2017, 2018, 2019 and 2020. The upper panel shows the western region (Kongsbreen and Kronebreen glaciers), the bottom panel show the eastern region (Hinlopenbreen glacier). Note that the data contain manual corrections of falsely classified pixels and may contain inaccuracies. Also note the different time scales on the x-axes.

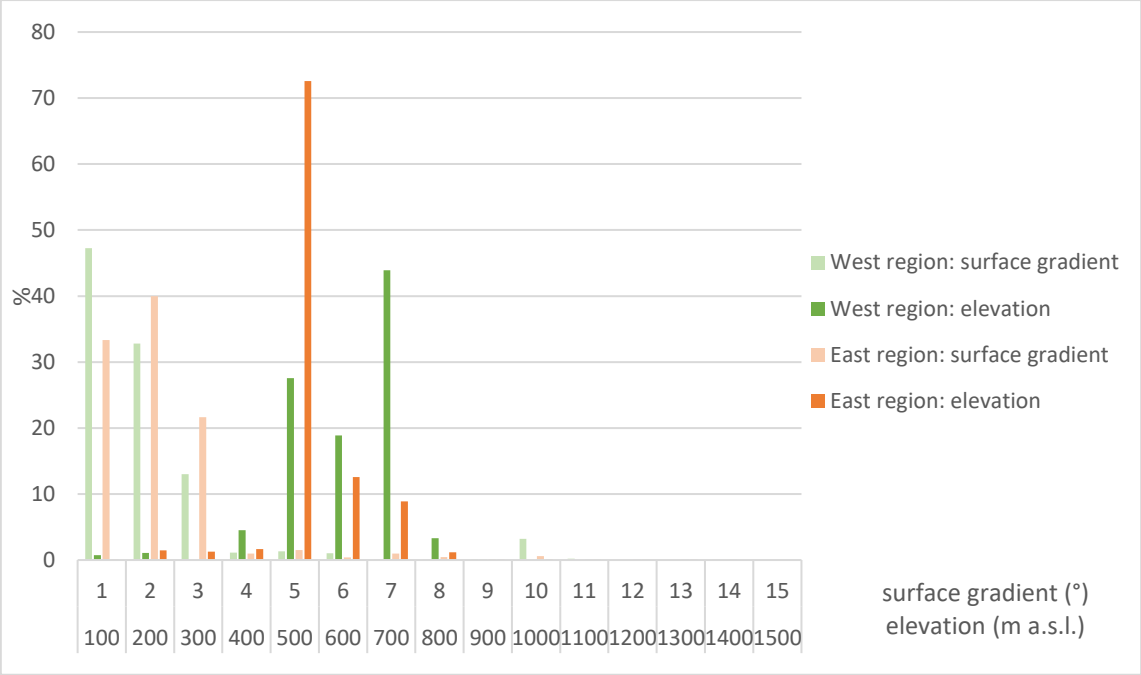

Figure 30 – Comparison of supraglacial lake distribution between the west region (2019) and east region (2018).

8. DISCUSSION

8.1. Temperature measurements

The fact that the mean summer temperature above Hinlopenbreen is higher than the mean summer temperature of Kongsbreen and Kronebreen was not in agreement with the original assumption that the west coast is under influence of the West Spitsbergen Current, thus warmer. The influence of the West Spitsbergen Current is highly visible on the southwest coast of Svalbard (see Figure 5 in Chapter 2.2.2.1.), however, the influence so far north is not as large as expected. The influence of the West Spitsbergen Current may be further diminished by the fact that the Kongsbreen and Kronebreen glaciers terminate at the easternmost part of the Kongsfjord fjord, about 30 km inland. Also, the island of Prins Karls Forland is located in front of the mouth of Kongsfjord, limiting the access of warm air into the fjord.

8.2. Image classification

The trends such as the beginning or the peak of the ablation season were analyzed based on data from the years 2017, 2018, 2019 and 2020. A semi-automated classification method based on the NDWI was used, which was partly successful. The evaluation was done by visual comparison of the results and the RGB composites shown in natural colors. With the threshold of 0.9 water was successfully distinguished from snow and using the Brand-Cohen-Yang cloud detection method, cloud pixels were successfully eliminated. However, the attempt to separate water, slush and shadow pixels failed.

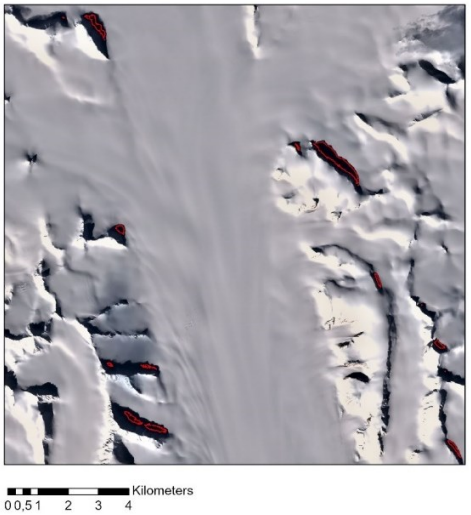

Figure 31 - Shadows misclassified as water on Kronebreen, 6.5.2017 (Sentinel-2).

Previous studies focused on the of mapping supraglacial hydrology on the Greenland Ice Sheet or in Antarctica (Yang, Smith 2013; Moussavi et al., 2020; Stokes et al., 2019). Yang and Smith (2013) used WorldView-2 imagery to delineate supraglacial meltwater channels in southwestern Greenland based on the $NDWI_{ice}$ (computed using the red and green bands) and came to a similar result, namely that the index *"only partially discerns slush from liquid water and may completely fail in very wet and/or saturated areas"*. They tried to solve the problem by creating more thresholds, however they were not able to completely prevent some slush areas from being misclassified as water.

The aim of this thesis was also to study the trends concerning the distribution of water and slush on the glacier surface. This was not feasible due to the number of manual corrections that needed to be made concerning areas of shadows falsely classified as water or slush. More investigation is needed for developing a method that will eliminate these areas from the classification. Most studies concerning on the topic of supraglacial hydrology have been conducted on the Greenland Ice Sheet, where no mountain ridges occur in the ablation zones as they do on the valley glaciers of Svalbard. Therefore, there is little need to address this problem. However, Hochreuter et al., (2021) looked for a solution as they found that in March/early May and in September/early October even small topographic features such as hills or crevasses cast shadows on the ice sheet surface. They used the R package "insol", the ArcticDEM with 10 m resolution and the sun position at the time of the image acquisition to create a mask of topographic shadows. This mask was then subtracted from the area of interest.

For this thesis, the results of the algorithm were visually compared with RGB composites and areas classified as water were manually corrected. After manual corrections of these areas, the differences were quantified (Table 5).

	2017		2018		2019		2020		overall	
T33XVH	9 685	36	8 317	268	6 785	44	8 497	73	8 115	104
T33XWH	14 746	39	15 026	124	13 918	226	2 680	226	14 430	117

Table 6 - Average area classified as water (in hectares) in different years. Left columns show values before manual corrections, right columns show values after manual corrections. The differences are very significant.

It was also found that the category 4 (vegetation/bare rock) was redundant, because the glacier outline of the Cryoclim "Glacier Area Outline" database cropped the area sufficiently. Also, the lower zenith angles in late September cause the snow to have a slightly orange or pink color,

causing large areas of snow to fall into category 4. However, since the comparison of the regions focused on supraglacial lakes, the categories of snow and vegetation/bare rock were not used further and the misclassification of snow into vegetation/bare rock did not anyhow affect the results.

8.3. Comparison of the study areas

Two types of comparison were conducted: one on the overall time trends during the ablation season, such as its beginning and peak, and one on the spatial distribution of supraglacial lakes. Due to insufficient cloud-free scenes available, two different ablation seasons were chosen for investigating the spatial distribution of supraglacial lakes, 2019 for the west region and 2018 for the east region. Having data from different ablation seasons is not entirely suitable for conducting a comparison, however, it is assumed that supraglacial lakes form in topographic depressions (Irvine-Fynn et al., 2017) each year and that the differences in their distribution will not be dramatic. It is important to note that the summer of 2019 was considerably warmer (Lindsey, 2019) and more melting could have occurred on the glacier. However, it was the best way to map the beginning and the peak of the ablation seasons for each region.

On average, the beginning and peak of the ablation seasons came about 10-days earlier in the west region than in the east region. That can be linked with the milder climate with higher average yearly temperatures in the west region (Copernicus Climate Change Service (C3S), 2021). Similarly, a *"2–3 week delay in the evolution of total supra-glacial lake area"* occurs in the northern areas of the Greenland Ice Sheet compared to the south-west, according to Sundal et al., (2009). In both regions, the onset of the melting corresponded temporally with the temperatures reaching positive values. With rising temperatures, lakes started appearing in higher elevations and the melting progressed further inland in both regions.

The date when the temperatures reach positive values and the melting begins possibly has a larger effect on the formation of supraglacial lakes than the actual course of temperatures throughout the ablation season. In the east region temperatures were persistently rising until the end of August, but the peak of the ablation season came on the 10th of July – approximately 20 days after the first supraglacial lakes appeared on the glacier surface. By the end August, when the highest temperatures were measured, most supraglacial lakes were already drained. Similarly, in the west region the peak of the ablation season also came approximately 20 days after the first supraglacial lakes formed. However, in the west region, the peak of the ablation

season came with the peak of the temperatures. According to measurements on a subpolar glacier in Svalbard made by Hagen in 1991 (Irvine-Fynn, 2017), supraglacial lakes persist on the glacier surface for 14 to 60 days. The results of this thesis correspond with this, however, the frequency of image availability over the study areas is not sufficient to determine the exact period for which a supraglacial lake persists on the glacier surface.

Supraglacial lakes are said to form in the ablation zone, under the equilibrium line, and according to Hanssen-Bauer et al. (2017) the equilibrium line was situated at about 600 m a.s.l. in the northeastern part of Svalbard and 850 m a.s.l. in the northwestern part between the years 1971 and 2000. It is projected to rise about 400 m higher until the year 2100.

Supraglacial lakes formed at higher elevations in the west region than in the east region, which corresponds with the distribution of the equilibrium line. At the Kongsbreen and Kronebreen glaciers (west region) supraglacial lakes were detected lower than 850 m a.s.l., which is below the estimated equilibrium line altitude (ELA). However, at the Hinlopenbreen glacier (east region) supraglacial lakes were detected in elevations between 600 and 700 m a.s.l. which may indicate a certain rise in the ELA, since the estimated ELA for this region is 600 m a.s.l. (Hanssen-Bauer et al., 2019). However, this would need a further study and comparison of older imagery, because no studies of this area have been conducted before. Since Sentinel-2 only orbits the Earth from 2016, the use of Landsat 8 imagery would be suitable for mapping the changes.

8.4. Further research

Another interesting aspect to study would be the lake volume, as it would enable the quantification meltwater runoff. A problematic aspect of this is that the measuring of lake volume would require *in situ* measurements (Dow et al., 2015; Fitzpatrick et al., 2014; Yang et al., 2019) for validating the results. However, there are also methods to estimate the lake volumes based on their albedo (Moussavi et al., 2020; Pope et al., 2016; Sneed, Hamilton 2007) and on the depth-albedo relationship.

The use of SAR imagery (Miles et al., 2017) should also be considered because it penetrates through snow and ice and can reveal snow-covered lakes that cannot be detected by the NDWI. Another advantage of radar imagery is that it penetrates through clouds and is not affected by

the atmospheric conditions. It could be used to study the lakes that persist even during the winter (Schröder et al., 2020; Miles et al., 2017).

9. CONCLUSIONS

For the purposes of this thesis an algorithm that detected water bodies on the glacier surface using Sentinel-2 imagery was developed. The classification was made using the normalized difference water index and the largest objective was to distinguish water bodies from slush zones and shadows, which was not fully successful, as it was necessary to make manual corrections.

The distribution of supraglacial lakes was mapped in two areas of Spitsbergen, the largest island of the Svalbard archipelago; the study area on the west coast contained the glaciers Kongsbreen and Kronebreen, and the study area on the east coast featured the glacier Hinlopenbreen. The former objective was to examine also the inter-annual differences, but this was not possible due to the lack of a sufficient temporal coverage of cloud-free scenes for each year. This can be a topic for further research, together with the analyzing of long-term trends and changes in the ablation season.

The beginning and peak of the ablation season occurred earlier in the west region than in the east region between the years 2017 and 2020. The beginning of the ablation season seemed to be a reaction to the temperatures reaching positive values, and the ablation peaked about 20 days after the first supraglacial lakes appeared. For the west region it was at the beginning of July, for the east region it was about 10-15 days later, similarly to the offset of the beginning of the ablation season.

At the beginning of the ablation season supraglacial lakes formed in lower elevations and with rising temperatures they progressively appeared in higher elevations. The most supraglacial lakes formed between 600 and 700 m a.s.l. in the west region and between 400 and 500 m a.s.l. in the east region. In both regions the supraglacial lakes formed in places with low surface gradients (<3°).

In the east region a large number of supraglacial lakes (12 % of the total lake area in the east region) formed above the estimated equilibrium line altitude (ELA) of 1971-2000, which poses a question whether the ELA is rising, and if so, how much. The inter-annual and long-term trends and changes could be a topic for further research in this field of study. The progressive rise of supraglacial lakes in elevation with rising temperatures indicates that a warming climate could move the supraglacial lakes into higher elevations. That could expand the area in which

connections between the glacier surface and the glacier bed form and could affect its dynamics. Larger areas of water on the glacier surface would also significantly affect the albedo, contributing to the positive feedback loop of glacier melt.

10. LITERATURE

AHLMANN, H. W. (1935): Contribution to the physics of glaciers. Geographic Journal, 86, 97–113.

ALLEN, H., DI LIBERTO, T., LINDSEY, M., LINDSEY, R., SCOTT, M. (2020): 2020 Arctic Report Card: Climate.gov visual highlights, Climate.gov, https://www.climate.gov/news-features/understanding-climate/2020-arctic-report-card-climategov-visual-highlights (4. 5. 2021).

ASCHWANDEN, A., FAHNESTOCK, M. A., TRUFFER, M., BRINKERHOFF, D. J., HOCK, R., KHROULEV, C., MOTTRAM, R., KHAN, S. A. (2019): Contribution of the Greenland Ice Sheet to sea level over the next millennium. Science Advances, 6, 5, eaav9396.

ARORA, M.: Piedmont glaciers. In: SINGH, V. P., SINGH, P., & HARITASHYA, U. K. (Eds.). (2011). Encyclopedia of Snow, Ice and Glaciers. Encyclopedia of Earth Sciences Series.

BRAATEN, J., COHEN, W., YANG, Z. (2015): Automated cloud and cloud shadow identification in Landsat MSS imagery for temperate ecosystems. Remote Sensing of Environment, 169, 128–138.

COMISO, J.C., PARKINSON, C.L., MARKUS, T., CAVALIERI, D.J., GERSTEN R. Current state of sea ice cover, NASA, https://earth.gsfc.nasa.gov/cryo/data/current-state-sea-ice-cover (13.4.2021)

Copernicus Climate Change Service (C3S) (2021): ERA5: Fifth generation of ECMWF atmospheric reanalysis of the global climate. Copernicus Climate Change Service Climate Data Store (CDS), https://cds.climate.copernicus.eu/cdsapp#!/home (6.2.2021).

CHU, V. (2014): Greenland ice sheet hydrology: A review. Progress in Physical Geography, 38, 19–54.

COULSON, S., FJELLBERG, A., DARIUSZ, bullet, GWIAZDOWICZ, J., LEBEDEVA, N., MELEKHINA, E., TORSTEIN, bullet, CHRISTER, S., BULLET, E., MARALDO, K., LADISLAV, bullet, BULLET, M., SCHATZ, H., RÜ, bullet, SCHMELZ, R., GEIR, bullet, BULLET, S., STUR, E., GWIAZDOWICZ, D., MIKO, L. (2013): Introduction of invertebrates into the High Arctic via imported soils: The case of Barentsburg in the Svalbard. Biological Invasions, 25, 1–5.

DALLMANN, W. K. (2015): Geoscience atlas of Svalbard. Oslo: Norwegian Polar Institute.

D'ANDREA, W., VAILLENCOURT, D., BALASCIO, N., WERNER, A., ROOF, S., RETELLE, M., BRADLEY, R. (2012): Mild Little Ice Age and unprecedented recent warmth in an 1800 year lake sediment record from Svalbard. Geology, 40.

DICKSON, R., OSBORN, T., HURRELL, J. W., MEINCKE, J., BLINDHEIM, J., ÅDLANDSVIK, B., VINJE, T., ALEKSEEV, G., MASLOWSKI, W. (2000): The Arctic Ocean Response to the North Atlantic Oscillation. Journal of Climate, 13, 2671–2696.

DOBIŃSKI, W. (2020): Permafrost active layer. Earth-Science Reviews, 208, 103301.

D'ODORICO, P., HE, Y., COLLINS, S., DE WEKKER, S., ENGEL, V., FUENTES, J. (2013): Vegetation–microclimate feedbacks in woodland–grassland ecotones. Global Ecology & Biogeography, 22.

DOW, C. F., KULESSA, B., RUTT, I. C., TSAI, V. C., PIMENTEL, S., DOYLE, S. H., AS, D. van, LINDBÄCK, K., PETTERSSON, R., JONES, G. A., HUBBARD, A. (2015): Modeling of subglacial hydrological development following rapid supraglacial lake drainage. Journal of Geophysical Research: Earth Surface, 6, 120, 1127–1147.

ELVEVOLD, S., DALLMANN, W. K., BLOMEIER, D. (2007): Geology of Svalbard. Tromsø: Norsk Polarinstitutt.

FARINOTTI, D., HUSS, M., FÜRST, J. J., LANDMANN, J., MACHGUTH, H., MAUSSION, F., PANDIT, A. (2019): A consensus estimate for the ice thickness distribution of all glaciers on Earth. Nature Geoscience, 3, 12, 168–173.

FITZPATRICK, A. a. W., HUBBARD, A. L., BOX, J. E., QUINCEY, D. J., VAN AS, D., MIKKELSEN, A. P. B., DOYLE, S. H., DOW, C. F., HASHOLT, B., JONES, G. A. (2014): A decade (2002–2012) of supraglacial lake volume estimates across Russell Glacier, West Greenland. The Cryosphere, 1, 8, 107–121.

FOUNTAIN, A. (2011): Temperate Glaciers. In: Singh, V. P., Singh, P., Haritashya, U. K. (eds.): Encyclopedia of Snow, Ice and Glaciers. Springer Netherlands, Dordrecht, 1145–1145.

GLASSER, N. F.: Polythermal glaciers. In: SINGH, V. P., SINGH, P., & HARITASHYA, U. K. (Eds.). (2011). Encyclopedia of Snow, Ice and Glaciers. Encyclopedia of Earth Sciences Series.

GROSVIK, B., PROKHOROVA, T., ERIKSEN, E., KRIVOSHEYA, P., HORNELAND, P., PROZORKEVICH, D. (2018): Assessment of Marine Litter in the Barents Sea, a Part of the Joint Norwegian–Russian Ecosystem Survey. Frontiers in Marine Science, 5.

HAEBERLI, W.: Glacier mass balance in SINGH, V. P., SINGH, P., & HARITASHYA, U. K. (Eds.). (2011). Encyclopedia of Snow, Ice and Glaciers. Encyclopedia of Earth Sciences Series.

HAGEN, J. O., LIESTOL, O., ROLAND, E., JORGENSEN, T. eds. (1993): Glacier atlas of Svalbard and Jan Mayen. Oslo: Norsk Polarinstitutt.

HAGEN, J.O., BARR S., (2019): Kronebreen, Store norske leksikon, https://snl.no/Kronebreen (23.4.2021).

HAGEN, J. O. (2020): Hinlopenbreen. Store norske leksikon. http://snl.no/Hinlopenbreen (23.4.2021).

HANSEN, J. R., HANSSON, R., NORRIS, S. (1996): The State of the Arctic Environment. European Environment Agency.

HANSSEN-BAUER, I., FØRLAND, E., HISDAL, H., MAYER, S., SANDØ, A., SORTEBERG, A., ADAKUDLU, M., ANDRESEN, J., BAKKE, J., BELDRING, S., BENESTAD, R., VAN DER BILT, W., BOGEN, J., BORSTAD, C., BREILI, K., BREIVIK, O., BØRSHEIM, K., CHRISTIANSEN, H., DOBLER, A., WONG, W. (2019): Climate in Svalbard 2100 - a knowledge base for climate adaptation. The Norwegian Centre for Climate Services.

HJELLE, A. (1993): Geology of Svalbard. Oslo: Norsk Polarinstitutt.

HISDAL, V. (1998): Svalbard Nature and History. Oslo: Norsk Polarinstitutt.

HOCK, R. (2005): Glacier melt: a review of processes and their modelling. Progress in Physical Geography: Earth and Environment, 3, 29, 362–391.

HOCK, R. (2010): Glacier Mass Balance. https://glaciers.gi.alaska.edu/sites/default/files/mccarthy/Notes_massbal_Hock.pdf (4.5.2021)

HODGKINS, R. (1997): Glacier hydrology in Svalbard, Norwegian high arctic. Quaternary Science Reviews, 9, 16, 957–973.

HOCHREUTHER, P., NECKEL, N., REIMANN, N., HUMBERT, A., BRAUN, M. (2021): Fully Automated Detection of Supraglacial Lake Area for Northeast Greenland Using Sentinel-2 Time-Series. Remote Sensing, 2, 13, 205.

HUMLUM, O., INSTANES, A., SOLLID, J. L. (2003): Permafrost in Svalbard: a review of research history, climatic background and engineering challenges. Polar Research, 2, 22, 191–215.

IRVINE-FYNN, T. D. L., HODSON, A. J., MOORMAN, B. J., VATNE, G., HUBBARD, A. L. (2011): Polythermal Glacier Hydrology: A Review. Reviews of Geophysics, 4, 49.

ISAKSSON, E., HERMANSON, M., HICKS, S., IGARASHI, M., KAMIYAMA, K., MOORE, J., MOTOYAMA, H., MUIR, D., POHJOLA, V., VAIKMÄE, R., VAN DE WAL, R. S. W., WATANABE, O. (2003): Ice cores from Svalbard—useful archives of past climate and pollution history. Physics and Chemistry of the Earth, Parts A/B/C, 28, 28, 1217–1228.

JENKINS, A.: Ice shelf. In: SINGH, V. P., SINGH, P., & HARITASHYA, U. K. (Eds.). (2011). Encyclopedia of Snow, Ice and Glaciers. Encyclopedia of Earth Sciences Series.

KÖNIG, M., KOHLER, J., & NUTH, C. (2013). Glacier Area Outlines - Svalbard [Data set]. Norwegian Polar Institute. https://doi.org/10.21334/npolar.2013.89f430f8

KOTTEK, M., GRIESER, J., BECK, C., RUDOLF, B., RUBEL, F. (2006): World Map of the Köppen-Geiger climate classification updated. Meteorologische Zeitschrift, 3, 15, 259–263.

LI, J., ROY, D. P. (2017): A Global Analysis of Sentinel-2A, Sentinel-2B and Landsat-8 Data Revisit Intervals and Implications for Terrestrial Monitoring. Remote Sensing, 9, 9, 902.

LIND, S., INGVALDSEN, R., FUREVIK, T. (2018): Arctic warming hotspot in the northern Barents Sea linked to declining sea-ice import. Nature Climate Change, 8.

LINDSEY, R. (2019): 2019 Arctic Report Card: Period of record and near-record warmth continues for sixth straight year, Climate.gov, https://www.climate.gov/news-features/featured-images/2019-arctic-report-card-melt-season-greenland-ice-sheet-rivals-record (4. 5. 2021).

LINDSEY, R. (2021): Climate Change: Global Sea Level, Climate.gov, https://www.climate.gov/news-features/understanding-climate/climate-change-global-sea-level (27. 4. 2021).

MANN, M. E., ZHANG, Z., RUTHERFORD, S., BRADLEY, R. S., HUGHES, M. K., SHINDELL, D., AMMANN, C., FALUVEGI, G., NI, F. (2009): Global Signatures and Dynamical Origins of the Little Ice Age and Medieval Climate Anomaly | Science. Science, 5957, 326, 1256–1260.

MILES, K. E., WILLIS, I. C., BENEDEK, C. L., WILLIAMSON, A. G., TEDESCO, M. (2017): Toward Monitoring Surface and Subsurface Lakes on the Greenland Ice Sheet Using Sentinel-1 SAR and Landsat-8 OLI Imagery. Frontiers in Earth Science, 5.

MORLIGHEM, M., WILLIAMS, C. N., RIGNOT, E., AN, L., ARNDT, J. E., BAMBER, J. L., CATANIA, G., CHAUCHÉ, N., DOWDESWELL, J. A., DORSCHEL, B., FENTY, I., HOGAN, K., HOWAT, I., HUBBARD, A., JAKOBSSON, M., JORDAN, T. M., KJELDSEN, K. K., MILLAN, R., MAYER, L., MOUGINOT, J., NOËL, B. P. Y., O'COFAIGH, C., PALMER, S., RYSGAARD, S., SEROUSSI, H., SIEGERT, M. J., SLABON, P., STRANEO, F., VAN DEN BROEKE, M. R., WEINREBE, W., WOOD, M., ZINGLERSEN, K. B. (2017): BedMachine v3: Complete Bed Topography and Ocean Bathymetry Mapping of Greenland From Multibeam Echo Sounding Combined With Mass Conservation. Geophysical Research Letters, 21, 44, 11,051-11,061.

MOUSSAVI, M., POPE, A., HALBERSTADT, A. R. W., TRUSEL, L. D., CIOFFI, L., ABDALATI, W. (2020): Antarctic Supraglacial Lake Detection Using Landsat 8 and Sentinel-2 Imagery: Towards Continental Generation of Lake Volumes. Remote Sensing, 1, 12, 134.

National Snow and Ice Data Center (2020a): Glacier Types: Icefields, https://nsidc.org/cryosphere/glaciers/gallery/icefields.html (20. 4. 2021).

National Snow and Ice Data Center (2020b): How are glaciers formed?, https://nsidc.org/cryosphere/glaciers/questions/formed.html (23. 4. 2021).

National Snow and Ice Data Center (2021): ice sheet. https://nsidc.org/cryosphere/glossary/term/ice-sheet (4.5.2021)

National Snow and Ice Data Center (2020c): Thermodynamics: Albedo. https://nsidc.org/cryosphere/seaice/processes/albedo.html (4.5.2021)

NOËL, B., JAKOBS, C. L., VAN PELT, W. J. J., LHERMITTE, S., WOUTERS, B., KOHLER, J., HAGEN, J. O., LUKS, B., REIJMER, C. H., VAN DE BERG, W. J., VAN DEN BROEKE, M. R. (2020): Low elevation of Svalbard glaciers drives high mass loss variability. Nature Communications, 1, 11, 4597.

NORDLI, Ø., PRZYBYLAK, R., OGILVIE, A. E. J., ISAKSEN, K. (2014): Long-term temperature trends and variability on Spitsbergen: the extended Svalbard Airport temperature series, 1898–2012. Polar Research, 1, 33, 21349.

Norsk Klimaservicesenter (n.d.): https://seklima.met.no/observations/ (6. 12. 2020).

Norwegian Meteorological Institute (n.d.): Ice Service charts:, https://cryo.met.no/en/latest-ice-charts (15. 12. 2020).

Norwegian Polar Institute (2014). Kartdata Svalbard 1:1 000 000 (S1000 Kartdata) [Data set]. Norwegian Polar Institute. https://doi.org/10.21334/npolar.2014.63730e2e

OPPENHEIMER, M., B.C. GLAVOVIC , J. HINKEL, R. van de WAL, A.K. MAGNAN, A. ABD-ELGAWAD, R. CAI, M. CIFUENTES-JARA, R.M. DECONTO, T. GHOSH, J. HAY, F. ISLA, B. MARZEION, B. MEYSSIGNAC, AND Z. SEBESVARI (2019): Sea level rise and implications for low-lying islands, coasts and communities. In: IPCC Special Report on the Ocean and Cryosphere in a Changing Climate [H.-O. Pörtner, D.C. Roberts, V. Masson-Delmotte, P. Zhai, M. Tignor, E. Poloczanska, K. Mintenbeck, A. Alegría, M. Nicolai, A. Okem, J. Petzold, B. Rama, N.M. Weyer (eds.)]. In press.

PELT, W. J. J. van, KOHLER, J., LISTON, G. E., HAGEN, J. O., LUKS, B., REIJMER, C. H., POHJOLA, V. A. (2016): Multidecadal climate and seasonal snow conditions in Svalbard. Journal of Geophysical Research: Earth Surface, 11, 121, 2100–2117.

PITCHER, L. H., SMITH, L. C. (2019): Supraglacial Streams and Rivers. Annual Review of Earth and Planetary Sciences, 1, 47, 421–452.

POPE, A., SCAMBOS, T. A., MOUSSAVI, M., TEDESCO, M., WILLIS, M., SHEAN, D., GRIGSBY, S. (2016): Estimating supraglacial lake depth in West Greenland using Landsat 8 and comparison with other multispectral methods. The Cryosphere, 1, 10, 15–27.

PORTER, C., MORIN, P., HOWAT, I., NOH, M.-J., BATES, B., PETERMAN, K., KEESEY, S., SCHLENK, M., GARDINER, J., TOMKO, K., WILLIS, M., KELLEHER, C., CLOUTIER, M., HUSBY, E., FOGA, S., NAKAMURA, H., PLATSON, M., WETHINGTON, JR. M., WILLIAMSON, C., BAUER, G., ENOS, J., ARNOLD, G., KRAMER, W., BECKER, P., DOSHI, A., D'SOUZA, C., CUMMENS, P., LAURIER, F., BOJESEN, M. (2018): "ArcticDEM", https://doi.org/10.7910/DVN/OHHUKH, Harvard Dataverse, V1, (3.3.2021).

RAVINDRA, R., CHATURVEDI, ARUN: Antarctica. In: SINGH, V. P., SINGH, P., & HARITASHYA, U. K. (Eds.). (2011). Encyclopedia of Snow, Ice and Glaciers. Encyclopedia of Earth Sciences Series.

REYNOLDS, J. M. (2000): On the formation of supraglacial lakes on debris- covered glaciers. IAHS publication, 264, 2000, 153–161.

RIGNOT, E., MOUGINOT, J., SCHEUCHL, B., BROEKE, M. van den, WESSEM, M. J. van, MORLIGHEM, M. (2019): Four decades of Antarctic Ice Sheet mass balance from 1979–2017. Proceedings of the National Academy of Sciences, 4, 116, 1095–1103.

SCHRÖDER, L., NECKEL, N., ZINDLER, R., HUMBERT, A. (2020): Perennial Supraglacial Lakes in Northeast Greenland Observed by Polarimetric SAR. Remote Sensing, 17, 12, 2798.

SHRESTHA, A.B.: Climate change and glaciers. In: SINGH, V. P., SINGH, P., & HARITASHYA, U. K. (Eds.). (2011). Encyclopedia of Snow, Ice and Glaciers. Encyclopedia of Earth Sciences Series.

SINGH, P. (2001): Snow and Glacier Hydrology. Springer Science & Business Media.

SINGH, V. P., SINGH, P., HARITASHYA, U. K. eds. (2011): Encyclopedia of Snow, Ice and Glaciers. Springer Netherlands, Dordrecht.

SNAP - ESA Sentinel Application Platform v2.0.2, http://step.esa.int

SNEED, W. A., HAMILTON, G. S. (2007): Evolution of melt pond volume on the surface of the Greenland Ice Sheet. Geophysical Research Letters, 3, 34.

STOKES, C. R., SANDERSON, J. E., MILES, B. W. J., JAMIESON, S. S. R., LEESON, A. A. (2019): Widespread distribution of supraglacial lakes around the margin of the East Antarctic Ice Sheet. Scientific Reports, 1, 9, 13823.

SUNDAL, A. V., SHEPHERD, A., NIENOW, P., HANNA, E., PALMER, S., HUYBRECHTS, P. (2009): Evolution of supra-glacial lakes across the Greenland Ice Sheet. Remote Sensing of Environment, 10, 113, 2164–2171.

SVENDSEN, J., MANGERUD, J. (1997): Holocene glacial and climatic variations on Spitsbergen, Svalbard. Holocene, 7, 45–57.

SYNEK, J., PETRÁNEK, J., SMETANA, V. (2007): ledovec. On-line Geologická encyklopedie. http://www.geology.cz/aplikace/encyklopedie/term.pl?ledovec (3.5.2021)

THE EUROPEAN SPACE AGENCY (2021): Sentinel-2 – Missions, https://sentinel.esa.int/web/sentinel/missions/sentinel-2 (4. 5. 2021).

USGS (): Landsat 8, https://www.usgs.gov/core-science-systems/nli/landsat/landsat-8?qt-science_support_page_related_con=0#qt-science_support_page_related_con (23. 4. 2021).

THOMAS, D., FOGG, G., CONVEY, P., FRITSEN, C., GILI, J.-M., GRADINGER, R., LAYBOURN-PARRY, J., REID, K., WALTON, D. (2008): The Biology of Polar Regions. Oxford University Press.

VAN DER BILT, W. G. M., BAKKE, J., VASSKOG, K., D'ANDREA, W. J., BRADLEY, R. S., ÓLAFSDÓTTIR, S. (2015): Reconstruction of glacier variability from lake sediments reveals dynamic Holocene climate in Svalbard. Quaternary Science Reviews, 126, 201–218.

VARGO, L. J., ANDERSON, B. M., DADIĆ, R., HORGAN, H. J., MACKINTOSH, A. N., KING, A. D., LORREY, A. M. (2020): Anthropogenic warming forces extreme annual glacier mass loss. Nature Climate Change, 9, 10, 856–861.

VIKHAMAR-SCHULER, D., FØRLAND, E. J., LUTZ, J., GJELTEN, H. M. (2019): Evaluation of downscaled reanalysis and observations for Svalbard - Background report for Climate in Svalbard 2100. The Norwegian Centre for Climate Services.

YANG, K., SMITH, L. C. (2013): Supraglacial Streams on the Greenland Ice Sheet Delineated From Combined Spectral–Shape Information in High-Resolution Satellite Imagery. IEEE Geoscience and Remote Sensing Letters, 4, 10, 801–805.

YANG, K., SMITH, L. C., FETTWEIS, X., GLEASON, C. J., LU, Y., LI, M. (2019): Surface meltwater runoff on the Greenland ice sheet estimated from remotely sensed supraglacial lake infilling rate. Remote Sensing of Environment, 234, 111459.

ZEMP, M., GÄRTNER-ROER, I., NUSSBAUMER, S. U., BANNWART, J., RASTNER, P., PAUL, F., AND HOELZLE, M. (eds.) (2020), Global Glacier Change Bulletin No. 3 (2016-2017). World Glacier Monitoring Service, Zurich, Switzerland.

ZWALLY, H. J. (2002): Surface Melt-Induced Acceleration of Greenland Ice-Sheet Flow. Science, 5579, 297, 218–222.

11. APPENDIX

Supplement_1: Contains a PDF file of weighted rolling averages of Svalbard temperatures between the years 2016 and 2020. Based on data from the ERA5-Land dataset (Copernicus Climate Change Service (C3S), 2021).

Supplement_2: Contains a map series depicting the evolution of supraglacial lakes through the ablation season of 2018 for the east region (Hinlopenbreen glacier). The images are named in the following key: *Region_Date*.

Supplement_3: Contains a map series depicting the evolution of supraglacial lakes through the ablation season of 2019 for the west region (Kronebreen and Kongsbreen glaciers). The images are named in the following key: *Region_Date*.